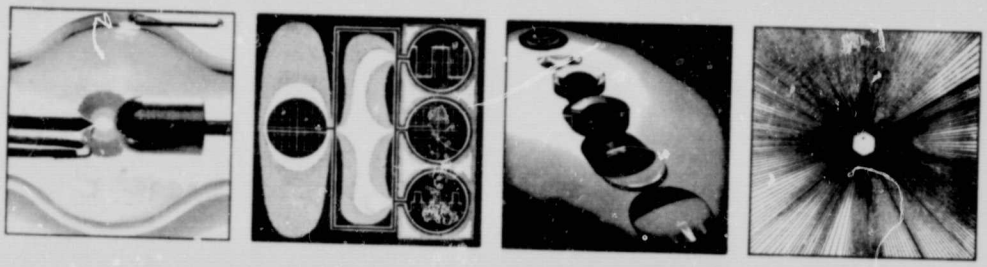

XEROX

NASA CR-159805

INERT GAS ION THRUSTER PROGRAM

PREPARED FOR

LEWIS RESEARCH CENTER

NATIONAL AERONAUTICS AND SPACE ADMINISTRATION

CONTRACT NO. NAS3-21345

Interim Report No. 1

March 1980

William Ramsey

Xerox Electro-Optical Systems

300 North Halstead Street
Pasadena, California 91107

CONTENTS

CONTENTS (contd)

ILLUSTRATIONS

SUMMARY

Tests were conducted with two existing magneto-electrostatic containment (MESC) ion thrusters: a 12-cm hexagonal (hex) and a 12-cm hemispherical (hemi). The former was designed and built by XEOS in 1968. The latter was developed for COMSAT in 1974 and loaned to XEOS for use in this program. The purpose of the tests was to evaluate and to optimize thruster performance using argon and xenon propellants. Operational tests of the 12-cm hex MESC ion thruster can be divided into three categories for discussion. First, the tests confirmed the excellent inert gas performance previously reported with the hex thruster. Second, the tests defined the optimum discharge chamber plasma operating parameters; and third, the tests investigated the interactions between the plasma parameters and hollow cathode subassembly. Results of the plasma/cathode investigation were used to select a cathode subassembly design for inert gas tests of the 12-cm hemispherical MESC thruster.

Hex MESC thruster tests achieved 79 percent argon mass utilization efficiency at discharge energy of 303 eV/ion and 90 percent xenon mass efficiency at 225 eV/ion. Optimum discharge chamber performance under mixed gas operation was achieved with argon hollow cathode flow and xenon main propellant flow. The xenon main flow configurations produced 92 percent ionic mass utilization at 220 eV/ion. The mass utilization efficiency and eV/ion figures mentioned above were corrected for neutral backflow from the vacuum system and doubly charged ion currents in the exhaust ion beam.

In the hex MESC thruster tests with different cathode magnets and baffles, changes in the cathode magnetic field and/or the cathode baffle affected thruster performance. Tests with the original cathode magnet and a keeper potential annular baffle reduced xenon discharge operating potential by 25 percent. Xenon annular baffle tests achieved 82 percent mass utilization at 260 eV/ion in a 29 volt discharge.

The 12-cm hemispherical MESC thruster tests showed an unexpected reduction in performance compared to that of the hex thruster. Preliminary performance mapping tests produced 67 percent argon mass utilization efficiency at 420 eV/ion and 90 percent xenon mass utilization at 389 eV/ion. The relatively poor hemi thruster inert gas performance was attributed to a shorter discharge chamber and a weaker, nonuniform peripheral magnetic field. This hypothesis was subsequently confirmed in a complementary IR&D program which showed hemispherical thruster performance could be improved by situating the boundary anodes in a more uniform magnetic field.

The on-going phase of this program is currently examining magnetic materials and configurations that will improve the uniformity and increase the magnetic field at the anodes. Proper magnet selection should improve hemi performance.

SECTION 1

INTRODUCTION

1.1 PROGRAM IDENTIFICATION AND PURPOSE

For electric propulsion application, high mass utilization and electrical efficiencies, high beam current densities, and long lifetimes are highly desirable. The MESC thruster design has provided the most promising inert gas ion source performance to date. Previous MESC thruster tests[1] indicated areas of thruster design, especially in the cathode region, which have potential for significant improvement.

The objective of this effort* was to advance the development of a high performance inert gas ion source suitable for both propulsive and non-propulsive users and to delineate performance characteristics for evaluating its full potential of application. The areas of effort were:

a. Cathode design and operating techniques
b. Reduction of wall losses in the plasma confinement region
c. Optimized operating regime in terms of source plasma density
d. Diagnostics measurements in the ion beam and the source plasma

Specifically, results from the 12 cm hex MESC thruster were used to design an inert gas cathode subassembly for the hemi thruster. The original cesium cathode of the COMSAT hemi thruster was not suitable for the inert gas operation. The hex and hemi thruster test results will be incorporated in the design of a third, improved MESC inert gas thruster in the next phase of the program.

---

*This work was performed under contract NAS3-21345, "Inert Gas Ion Thruster Development," administrated by NASA Lewis Research Center, Cleveland, Ohio

1.2 MESC OPERATING PRINCIPLES

The unique design of the MESC discharge chamber produces a highly ionized, uniform plasma with minimum discharge power consumption for a wide range of propellants. The efficient discharge operational characteristics are produced by crossed field (E x B) containment at the interface between the discharge plasma and chamber walls. Adjustment of the cross fields at the plasma periphery maximizes the electron diffusion path length for the operational characteristics of the selected propellant species. This approach increases the electron ionization efficiency and minimizes the discharge power consumption. The magnetic field free discharge volume produces a uniform plasma that provides the greatest extracted ion beam current density.

The peripheral crossed magnetic and electric fields are produced by alternate rings of anodes and magnets placed along the discharge chamber walls parallel to the grid system plane as shown in figure 1-1. The magnet rings are magnetized orthogonal to the walls and alternate in polarity from ring to ring to produce a strong magnetic field over the anodes, which cancels out in the chamber volume. Anode magnetic field adjustments are accomplished by radially repositioning the anodes. Figure 1-2 is a schematic of the typical MESC anode-magnet geometry, where B_p is the magnetic field at the magnet face, B_A the magnetic field over the anode, and E the anode electric field.

The cusp-shaped magnetic field along the chamber wall serves to contain the discharge plasma by modulating the electron diffusion current to the anodes and minimizing ionic recombination losses. The electron diffusion across a magnetic field was found to be directly proportional to the Maxwellian electron distribution temperature and inversely proportional to the magnetic flux density according to Bohm. Electron diffusion defined by this relationship was semi-empirically derived

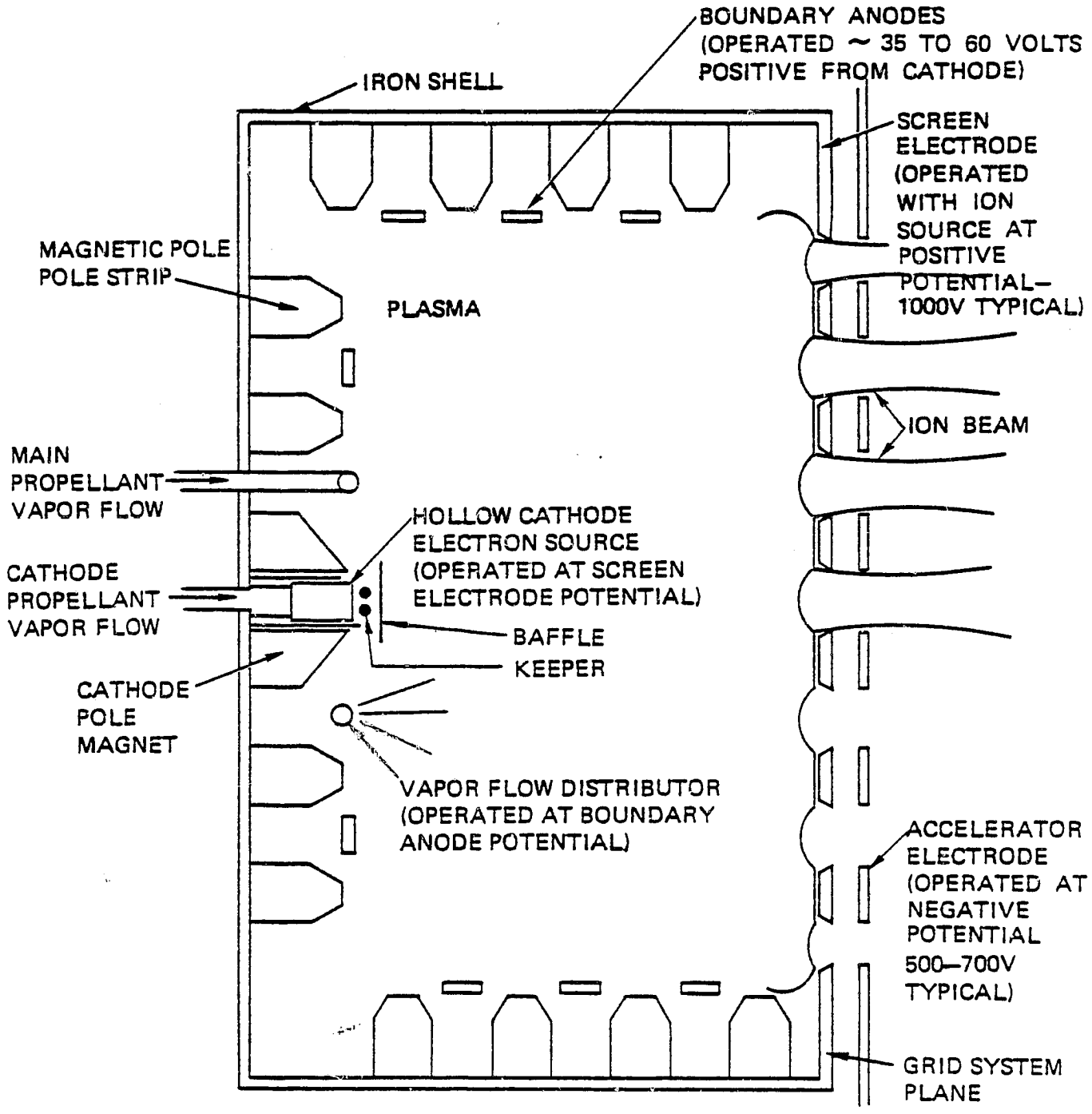

Figure 1-1. Cutaway Schematic of Hexagonal MESC Thruster

64840

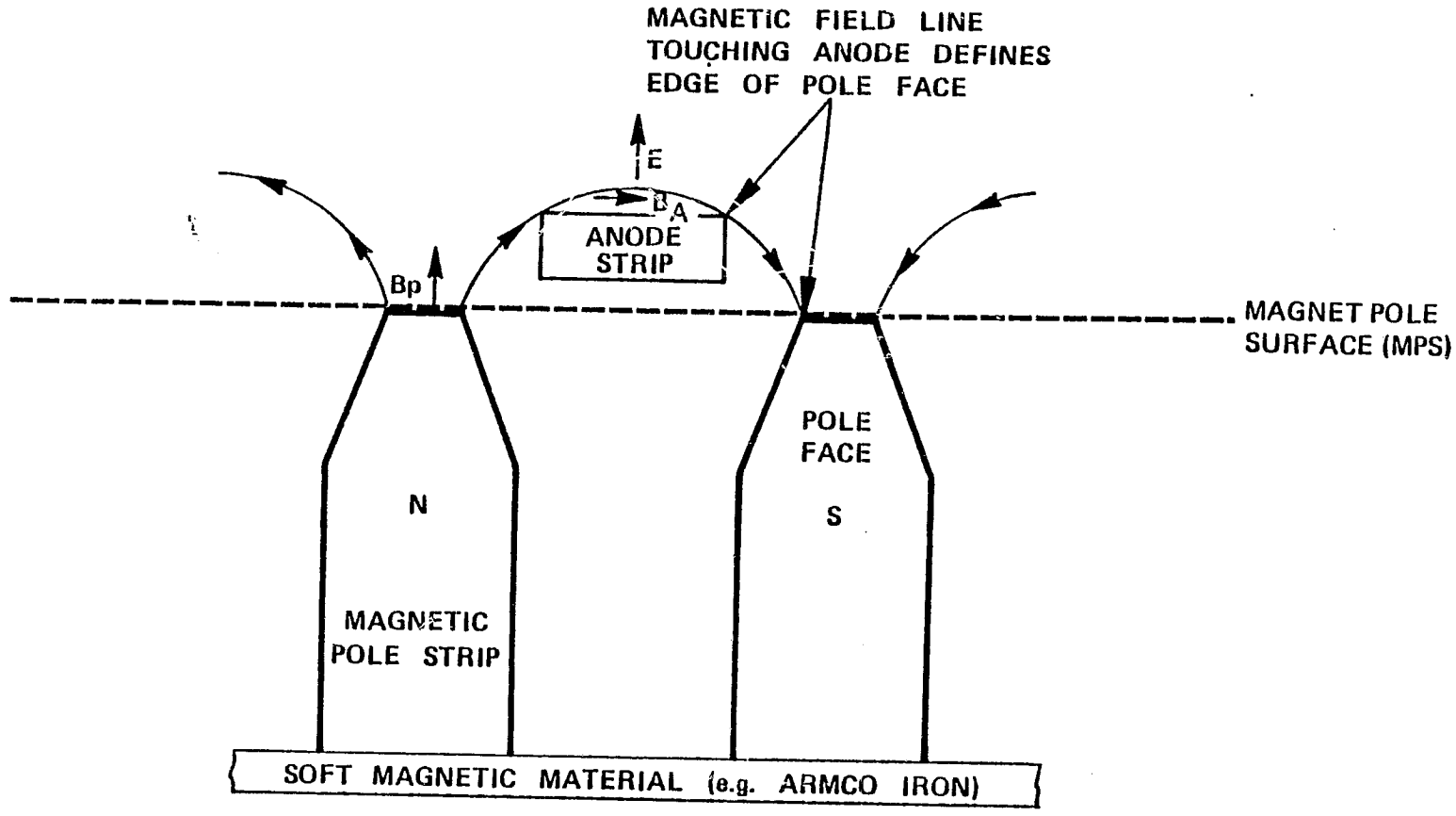

Figure 1-2. Basic MESC Anode-Magnet Configuration

from a fully ionized argon plasma operating under conditions similar to those found in an ion thruster. Chen[3] reports other workers confirmed Bohm's diffusion coeffieient and found that electron diffusion in regimes corresponding to ion thruster operation is also proportional to the plasma density gradient. The neoclassic Bohm diffusion referenced by Chen is:

$$D = \frac{1}{16} \frac{kT_e}{qB_A} \nabla n \qquad (1)$$

where:

- k = Boltzmann constant
- T_e = Maxwellian distribution electron temperature
- B_A = component of the magnetic field parallel to the discharge chamber walls
- q = electron charge
- ∇n = plasma density gradiant

The Maxwellian electron temperature, T_e, is the minimum energy an electron needs to diffuse to the anode. In a typical thruster discharge plasma, these lower energy electrons are present in order of magnitude greater concentrations than the high energy or primary electron and, therefore, have almost all the collisions in either classic[3] or neoclassic Bohm diffusion.

Kaufman[4] found Bohm diffusion should be further modified for multipole thruster application. Assuming zero electric field close to the anode and uniform density in the diffusion region, Kaufman showed the wall/anode diffusion current density is given by:

$$j \sim \frac{kT_e \, n_e}{13 \int B dx} \qquad (2)$$

where n_e is the electron density and $\int Bdx$ is the integrated flux density between magnet pole surface (MPS) and the field zero at the anode site midway between adjacent magnets. The magnetic pole surface is shown schematically in figure 1-2.

Robinson[5] showed the multipole magnetic field midway between magnets of opposite polarity is:

$$B = B_p \exp[-1.5\ (x/d + 0.5)^2] \qquad (3)$$

where:

B_p = magnetic field at the magnetic pole
x = displacement between the MPS and anode surface
d = center-to-center spacing of adjacent magnets

Typically, anodes in a MESC design thruster are located far from the MPS where $x > d$. Hence, B is a slowly varying function of x and $\int Bdx$ can be approximated with:

$$\int Bdx \sim B_A$$

where B_A is the field at the surface of the anode parallel to the chamber walls. Given the Maxwellian electron temperature and electron density in the discharge plasma, it is possible to adjust anode magnetic field for the optimum current density to a first approximation with the relationship:

$$j \propto \frac{kT_e}{B_A} n_e$$

The magnetic field-anode geometry also limits ionic recombination losses in the MESC discharge chamber. Using cusped field ion sources,

other workers[6] found the ionic recombination losses were inversely proportional to the magnetic field. Two investigators[7,8] independently determined ionic recombination losses were proportional to the square root of the product of primary electron and ionic Larmor radii or the "hybrid radius" defined by the following equation in MKS units:

$$p_x = \text{Larmor Radius} = \frac{m_x v_\perp}{q B_p} \quad (4)$$

$$\text{Hybrid Radius} = (p_i p_e)^{1/2} \quad (5)$$

where:

m_x = electron or ionic mass
$v_\perp$ = component of the velocity orthogonal to the magnetic field
q = electronic charge
B_p = magnetic field at the pole

In the hybrid radius definition, p_i and p_e are the electron and ion Larmor radii, respectively.

The hybrid radius was found[7,8] to be the width of the ion loss area at the magnet pole face along the discharge chamber walls, while the total ion loss region was the product of the magnet length and the radius. This relationship was found to apply to several gases under a wide range of operating conditions that included argon plasma at temperatures and densities similar to those found under nominal operation in an ion thruster.

In the MESC discharge chamber, the magnet surface exposed to the plasma is defined by the magnetic field lines connecting the magnet surface and the anode edges or critical field lines. The charged particles reaching these lines are collected at the anodes while those that do not are reflected or lost at the magnet surfaces defined by the

critical magnetic field lines and hybrid radius illustrated in figure 1-2. Increases in the magnet pole field strength cause the anodes to be located farther from the MPS to keep a constant magnetic flux density over the anodes surfaces and maintain the same plasma operating conditions. Thus, stronger magnets tend to reduce ion recombination losses by reducing the magnet pole face defined by the boundary geometry and the hybrid radius. Test results tend to support this model as will be discussed in later sections of this report.

1.3 INERT GAS MESC THRUSTER DEVELOPMENT PROGRAM

During the previous development program, under NASA contract NAS3-20393, the 12 cm MESC hexagonal discharge chamber[1] was modified for inert gas operation and performance mapped. The thruster achieved 81 percent argon mass efficiency and 96 percent xenon mass efficiency at 400 and 350 eV/ion, respectively. The discharge chamber performance with xenon cathode flow and argon main flow produced 76 percent mass utilization at 340 eV/ion.

The 12 cm hex thruster performance curves with argon and xenon are shown in figure 1-3. All performance values were corrected for ingestion of neutral backflow and double ion production. The sum of the keeper and main discharge power consumptions are used for computing performance. It can be seen in figure 1-3, hex thruster operational characteristics produced a change in the performance curve slope, "knee," at 74 percent argon mass utilization and 92 percent xenon mass utilization. Hence, the optimum hex thruster performance was achieved with a 315 eV/ion argon discharge producing mass utilization of 74 percent and a 225 eV/ion xenon discharge producing mass utilization of 92 percent.

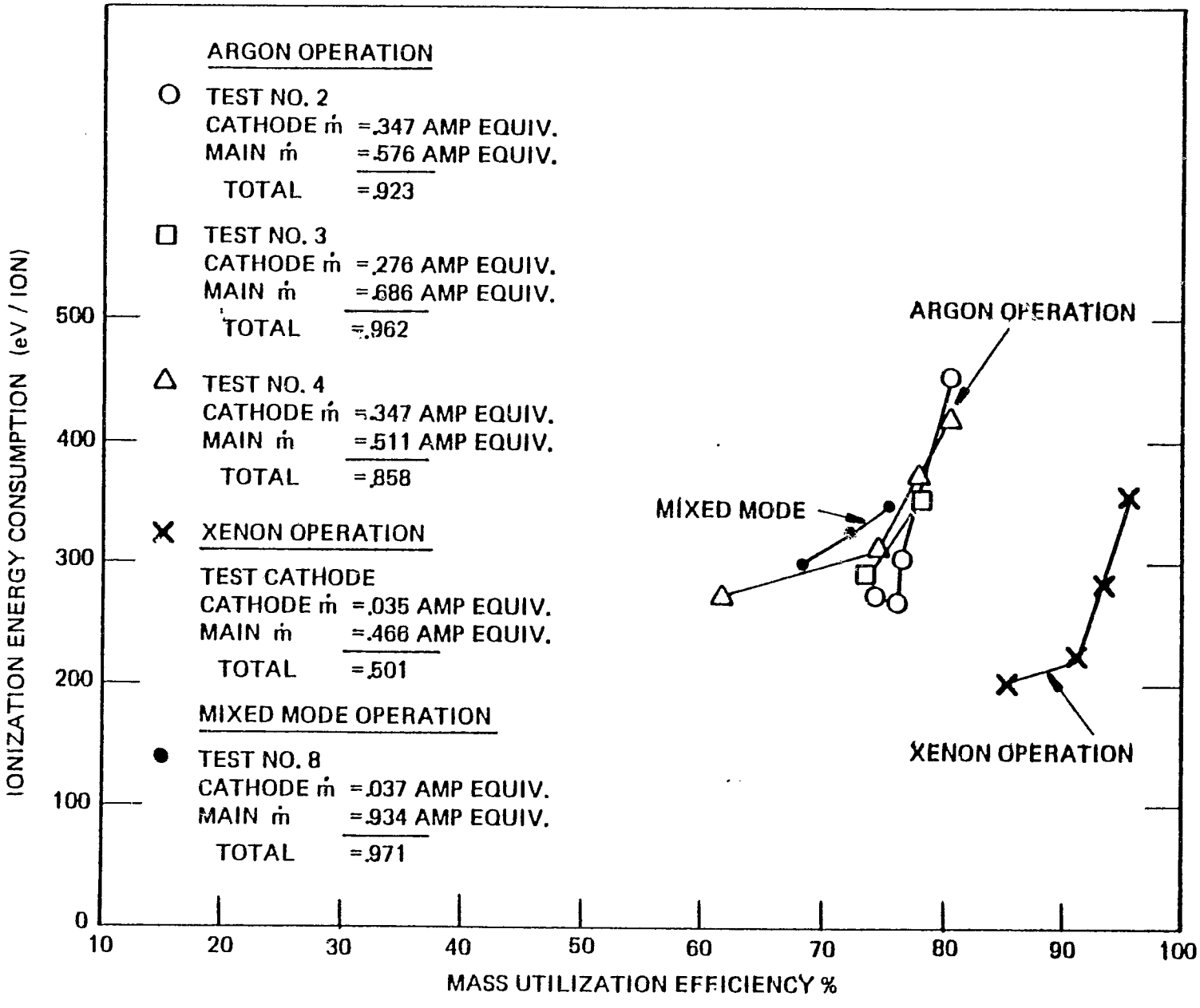

Figure 1-3. Hex Thruster Ionization Energy Consumption versus Mass Utilization Efficiency

1.4 GOALS OF THE SECOND INERT GAS MESC DEVELOPMENT PROGRAM

The work on this program was performed under NASA contract NAS3-21345 entitled, "Inert Gas Ion Thruster Development," which was administered by NASA Lewis Research Center, Cleveland, Ohio. The program had five primary goals: confirm the hex thruster inert gas performance; measure the discharge chamber plasma characteristics; observe how these characteristics are effected by hollow cathode design changes: apply hex thruster test results to hemi thruster inert gas modifications; and initiate hemi thruster performance tests. The method and and approaches used to accomplish these goals are discussed below.

The same hex thruster configuration tested during the previous program was retested with a discharge chamber Langmuir probe. Data were collected during the hex thruster tests with the original, baseline cathode and other hollow cathode subassemblies. Parametric thruster data and probe data were collected during tests with the baseline and several other cathode designs.

The hemi thruster was modified for inert gas operation without major structural changes and preliminary performance tests were conducted. Hemi and hex thruster tests were conducted over a similar range of operational parameters to evaluate the effects of discharge chamber shape on thruster performance.

1.5 REPORT ORGANIZATION

This report is divided into five sections. Section 2 describes the apparatus used in testing, and Section 3 presents the test results. The fourth and fifth sections discuss the applications of the observed test results and the conclusions that can be drawn from these results.

SECTION 2

TEST APPARATUS

2.1 OPTIMIZED 12 CM HEXAGONAL MESC INERT GAS ION THRUSTER

The hexagonal chamber was the first discharge chamber designed to use alternate rings of permanent magnets and anodes[9] to contain the plasma and control the electron diffusion currents to the boundary anodes. The hex shaped rings are positioned along the side and rear walls of the chamber with a hollow cathode subassembly extending through the rear wall on axis as shown in figure 2-1. Each of the hexagonal-shaped magnet rings is made up of six sections of AlNiCo material magnetized to 0.2 Tesla in a direction perpendicular to the chamber walls. Alternate magnet rings have opposite magnetic polarity. The hex-shaped rings along the walls produce a cusped-shaped peripheral magnetic field to contain the discharge plasma and control electron diffusion current to the interspersed anodes.

The anodes were U-channels that extended into the discharge. The sides of the channels were dimensioned to match inert gas operational characteristics and plasma densities found during testing. At the completion of hex thruster optimization, the magnetic field component parallel to the walls across the channels averaged 1.2×10^{-2} Tesla.

The optimized inert gas hexagonal MESC thruster was used to select a cathode subassembly design which fit the spacial limitation of the hemispherical thruster and maintained thermal isolation between the operating cathode and the heat sensitive permanent magnets. The hex thruster was a laboratory device that could be easily taken apart and and modified for certain changes in the cathode region. Removal of

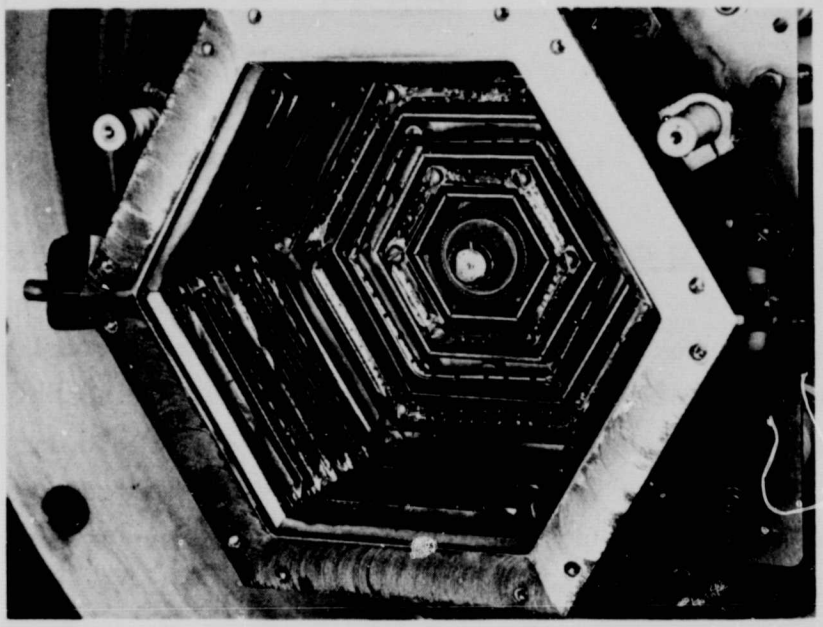

Figure 2-1. Downstream View of 12 cm Hexagonal MESC Thruster

the rear, or upstream, wall of the hex discharge chamber allowed access to the cathode and main feed introduction plenum. If the rear wall was removed, it was possible to substitute a larger cathode pole magnet for the existing one or modify the main feed introduction system. Without removing the rear wall, it was possible to change the cathode baffle, keeper, and cathode pole magnet.

2.1.1 CATHODE SUBASSEMBLIES

Five different cathode baffle magnet designs were tested in the hex thruster with a 3.2 mm diameter cathode. Each of the subassemblies was tested at the same mass flows in three operational modes: argon single gas discharge operation; xenon single gas discharge operation; and a discharge containing a mixture of argon and xenon or "mixed mode." The hex thruster original cathode assembly underwent testing with single gases and both possible mixed modes. Tests were conducted with the modified cathode baffle-magnet configurations in the single gas modes and argon cathode mixed mode with xenon gas main flow. Argon cathode mixed mode operation was selected for further testing as it produced the most promising performance with the hex thruster original cathode assembly.

The five cathode baffle-magnet designs can be divided into two distinctive types of subassemblies for discussion purposes. The first, smaller type could easily fit the dimensions of the original 2.3 diameter cathode pole magnet. The second type had a larger, 3.3 cm diameter, cathode pole magnet and baffle structure that would have necessitated major rework of the hemi discharge chamber.

The first smaller cathode subassembly tested was the original or baseline cathode depicted in figure 2-2. The baseline cathode was designed for the 2.3 cm diameter cathode pole magnet and had separate support

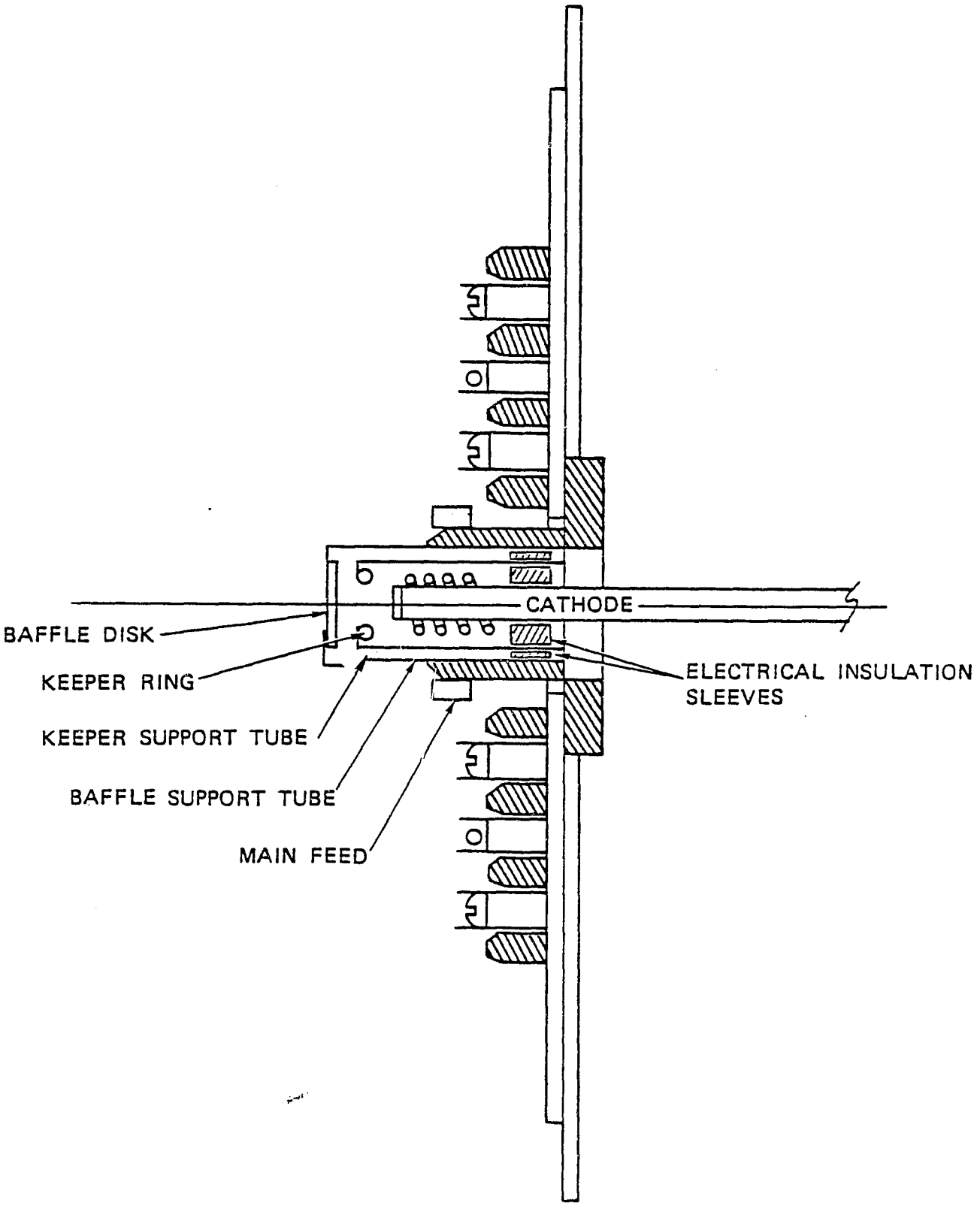

Figure 2-2. Cutaway Schematic of the Hexagonal Thruster Rear Wall with Baseline Cathode Magnet-Baffle

tubes for the baffle disk and the keeper ring. The keeper and baffle tubes were 1.1 and 1.6 cm diameter, respectively. The keeper ring and baffle disk were suspended from the tubes with 0.25 mm diameter tantalum wire as shown. Electrical isolation of the keeper tube was achieved with two boron nitride sleeves between the two support tubes.

In the next subassembly, shown in figure 2-3, the baffle and keeper support tubes were replaced with a single tube 1.3 cm diameter serving both functions. This design reduced the original cathode subassembly diameter 0.3 cm and biased the baffle tube to keeper potential. Tests were conducted with a 1.1 cm diameter solid baffle disk and an annulus baffle 1.3 cm diameter with an 0.8 cm centerline hole.

The single tube keeper potential subassembly was modified to accommodate a cathode radiating fin by increasing the diameter of the baffle-keeper tube to 1.9 cm downstream of the cathode magnet as shown in figure 2-4. The subassembly was fitted with an annular baffle 1.5 x 0.4 cm diameter during radiating cathode fin testing.

The second type of cathode subassembly required some modifications to the hex discharge chamber cathode regions and main gas flow lines. The 3.3 cm diameter cathode pole magnet was fitted in the discharge chamber by removing the main feed ring and using larger diameter baffle-keeper support tubes. The main gas flow was introduced into the discharge region through three anode potential tubes which penetrated every other section of the boundary anode adjacent to the cathode. The tubes were located 1.3 cm farther from the thruster centerline than the main feed plenum had been in the original design, as shown in figure 2-5.

The large cathode magnet tests were conducted with 1.3 cm diameter keeper support tube and a 1.9 cm diameter baffle support tube and a 1.5 x 0.42 cm annular baffle. The baffle tube was electrically

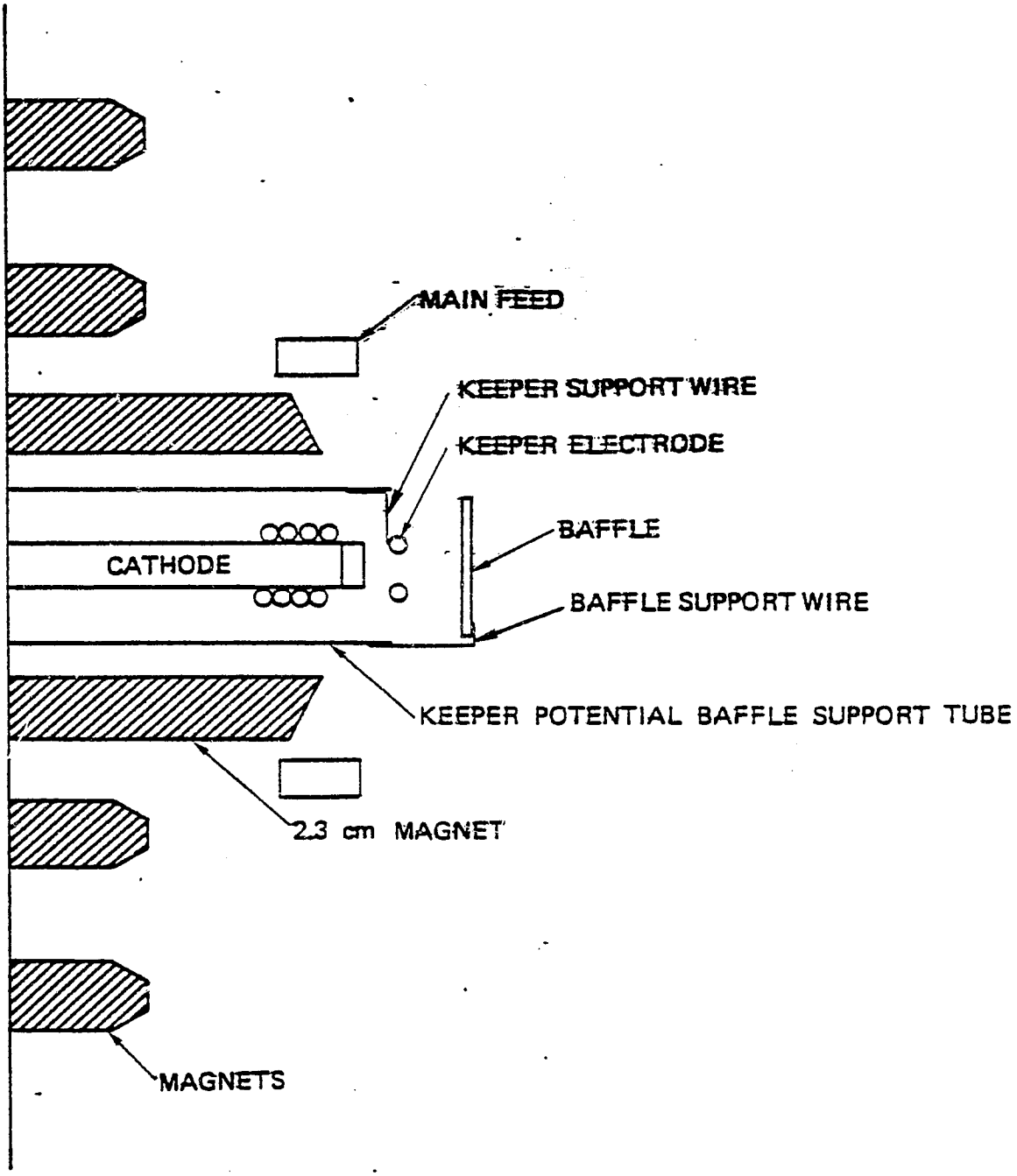

64819

Figure 2-3. Cutaway Schematic of 2.3 cm Magnet with Keeper Potential Baffle

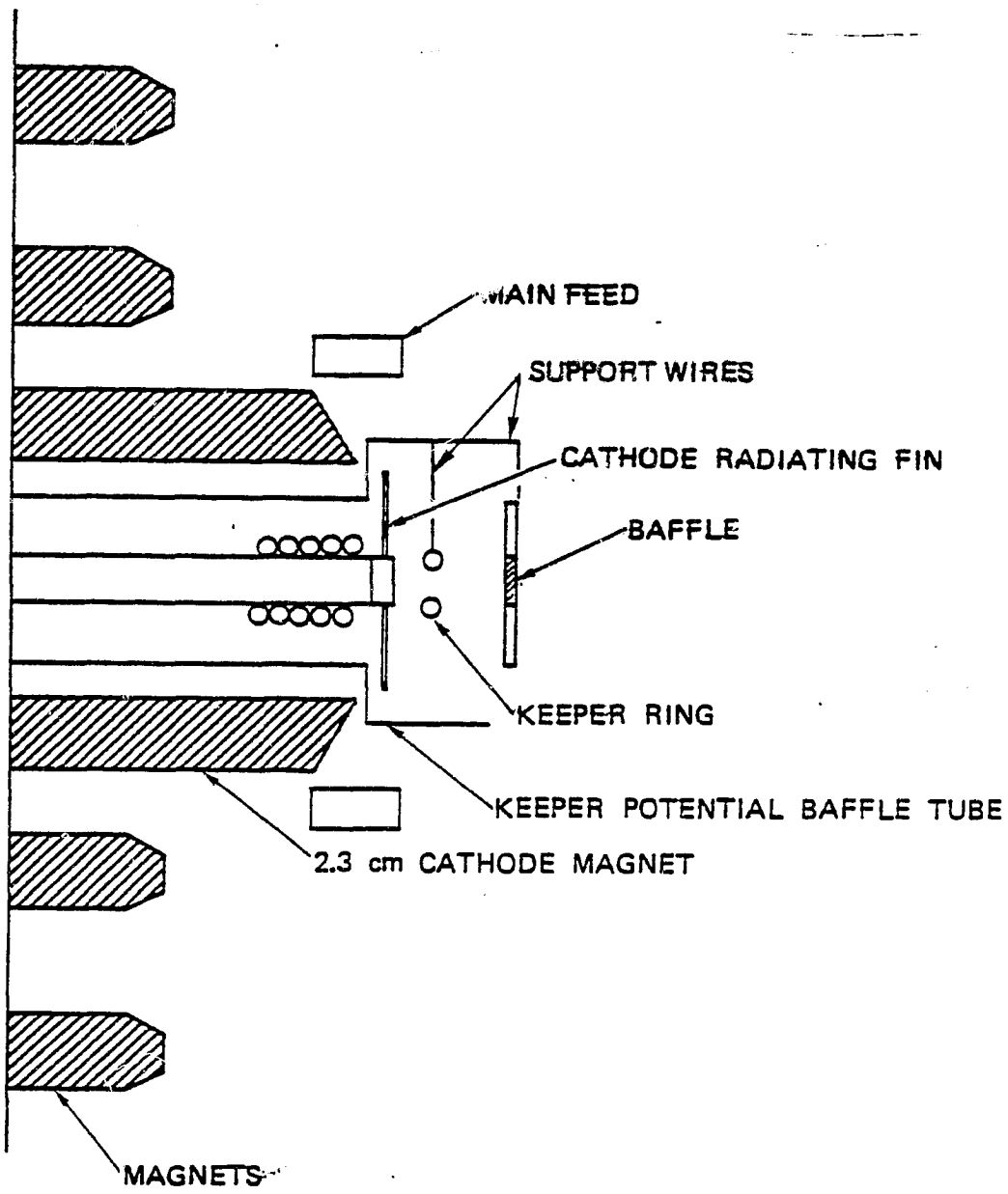

64821

Figure 2-4 Cutaway Schematic of 2.3 cm Magnet with Larger Diameter Keeper Potential Baffle

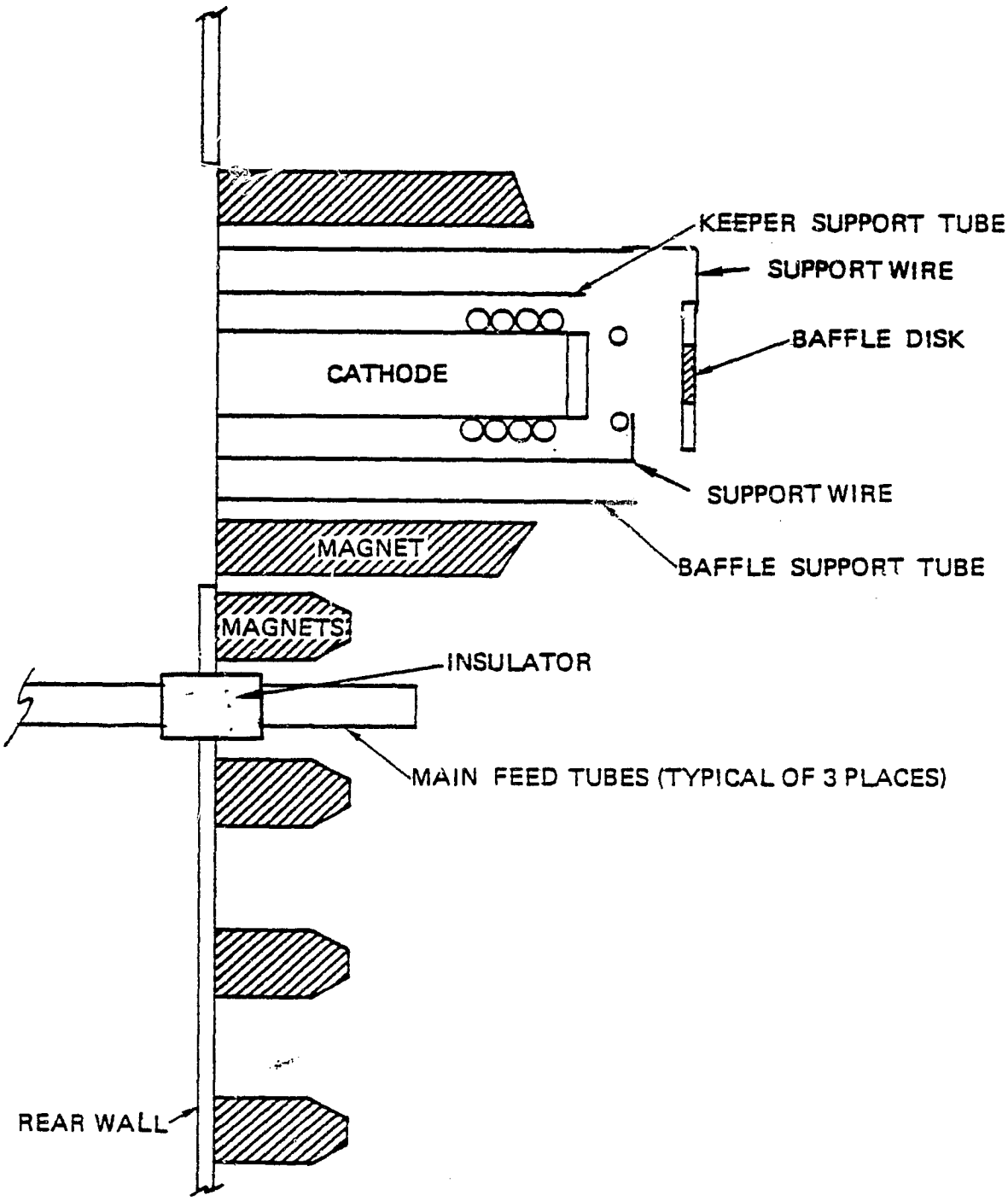

Figure 2-5. Cutaway Schematic of 3.3 cm Magnet Cathode Subassembly

isolated from the adjacent keeper and cathode potential hardware so it could be biased to any desired potential during testing.

The large diameter magnet subassembly shown in figure 2-5 provided greater thermal isolation between the cathode and pole magnet but increased the pole magnet size and ionic recombination area.

2.1.2 ION OPTICS

Two grid ion optics were used during all hex thruster tests.[1] The small-hole-accel (SHAG) type system consisted of a 69 percent geometric transparent screen and a 22 percent transparent accel with the same, uncompensated hexagonal hole pattern and different diameter holes. The transparency of the grids is a function of hole size and hole-to-hole spacing. The grids were fabricated from 0.25 mm thick molybdenum which was hydroformed into a 5.0 mm deep dish for thermal stability. The grids were dished downstream from the thruster with an intergrid gap of 1.0 mm.

2.1.3 GROUND SCREEN-NEUTRALIZER ASSEMBLY

During testing, the thruster was separated from the beam plasma with a 64 cm diameter ground potential cylinder made of stainless steel wire mesh and an annular downstream end cap. The ion beam exhausted through a 14 cm diameter hole in the end cap that exposed only accel potential hardware to the beam plasma. Stand-offs for the tantalum filament neutralizer were located on the perimeter of the ground screen hole beyond the edge of the typical beam spread.

2.2 THE 12 CM HEMISPHERICAL MESC THRUSTER

The 12 cm hemispherical MESC thruster was originally designed and built by XEOS for COMSAT as a flight prototype cesium ion thruster during a previous program.[10] Spaceflight requirements of minimum weight and structural integrity minimized flexibility and increased the difficulty of post-fabrication discharge chamber modification. Conversion from cesium to inert gas operation demanded several major changes in the discharge chamber design. A typical cesium discharge operated between 16 to 24 volts with a hollow cathode that was ignited and maintained without a keeper electrode or baffle structure. With this low plasma temperature and the hollow cathode operational mode, it was possible to use small, low mass, moderate field strength, high energy product (B x H) permanent magnets to contain the plasma and optimize the electron diffusion path to the anodes.

The hemi thruster MESC design consisted of platinum-cobalt magnet rings of opposite polarity interspersed with stainless steel anode rings. The transverse planes of the magnets and anodes were orthogonal to the hemi axis and decreased in diameter from the grid system mounting flange to the cathode. (See figure 2-6.) The magnetic circuit consisted of an ARMCO iron discharge chamber into which magnet locating grooves had been spun and 3.5 mm diameter Platcover magnets had been fitted. The magnet rings were split to fit into the grooves under compression and the gaps between the ends filled with a beryllium-copper plug to hold them in place. The Platcover rings were designed to be magnetized along hemispherical radii, that is, normal to the discharge chamber walls with a 0.15 Tesla residual field at saturation.

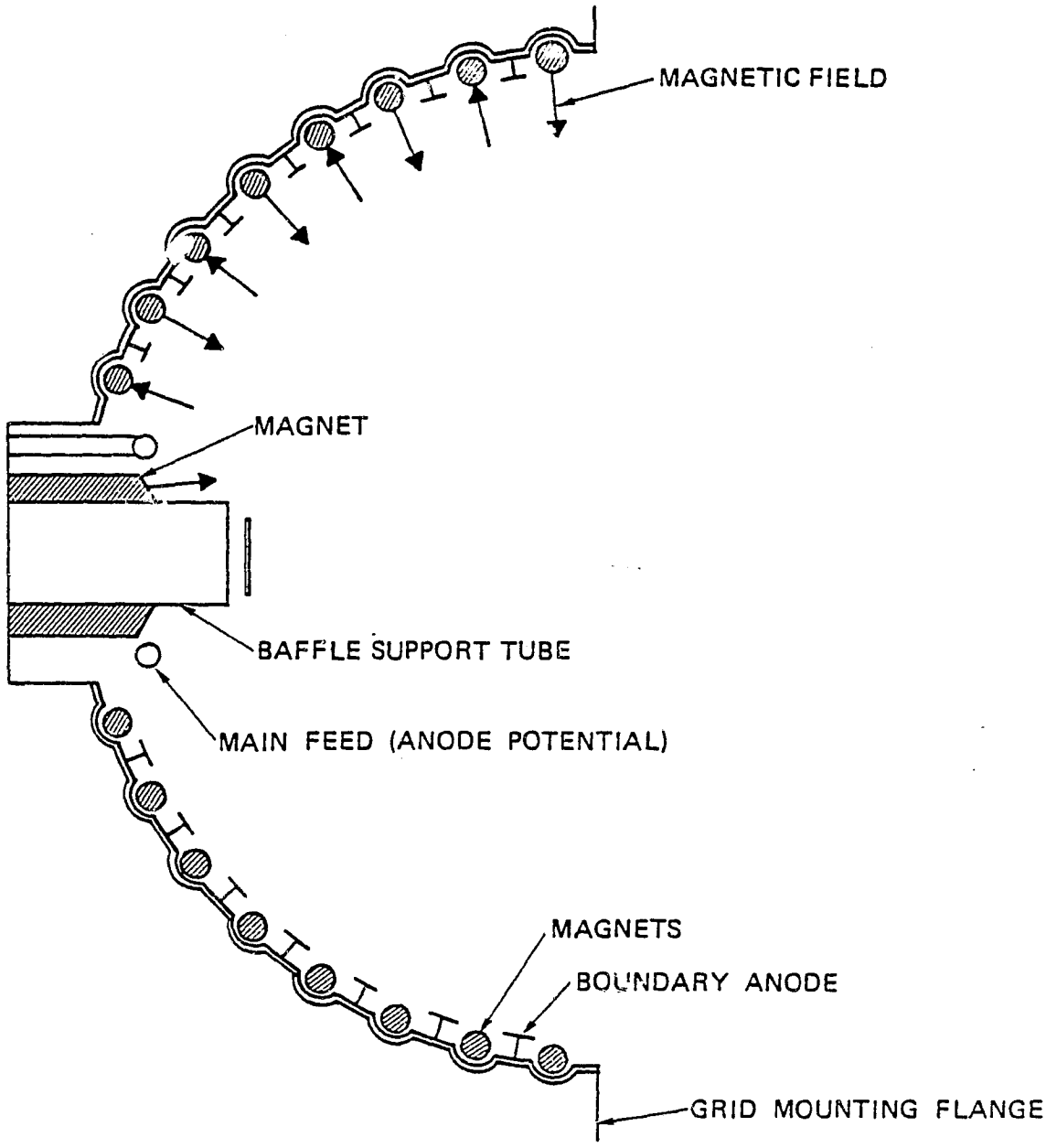

Figure 2-6. Cutaway Schematic of the Hemispherical MESC Discharge Chamber with Baseline Cathode Magnet-Baffle

64817

To convert the hemi thruster to inert gas operation, it was necessary to increase the magnetic field component parallel to the walls at the anodes and increase the physical size of the cathode magnet. The stronger peripheral field was needed to optimize the electron diffusion path with the higher temperature inert gas plasma. The larger cathode magnet was sized to fit the keeper electrode and baffle structure needed for efficient inert gas hollow cathode operation. A schematic of the inert gas test assembly is shown in figure 2-6.

2.2.1 HEMI THRUSTER BOUNDARY ANODES

Large differences in the anode magnetic field were noted when the anodes were being relocated for inert gas operation. This variation in the magnetic field close to the discharge chamber walls made it necessary to modify anode ring design to achieve the most efficient inert gas operation.

The peripheral magnetic field is an inverse square function of the anode-to-magnet displacement. The hexagonal thruster had a 10 percent point-to-point field variation along the majority of the anodes. By contrast, relocating the hemi thruster anodes at the calculated inert gas position produced an anode magnetic field that varied up to a factor of two between points azimuthally separated by 6 mm along a single anode surface. Further investigation found several sections of the Platcover rings had magnetic fields divergent from the normal to the wall by angles up to 30 degrees and large variations in flux density.

In order to fit the magnets into the grooves of the discharge chamber wall, the magnets had been fabricated up to 6.5 mm shorter than the groove length with a nonmagnetic beryllium-copper plug used to fill end gaps. When the anodes were located relatively far from the magnets

in the position for cesium operation, these deviations from nominal were averaged out to produce a 15 percent point-to-point variation in anode magnetic field. However, as the anodes were brought closer to the magnets for the inert-gas operation, the impact of these variations increased causing the wide swings in anode magnetic field.

Several actions were taken to minimize the effects of the magnetic field variation on thruster operation. First, the beryllium-copper plugs in the larger diameter magnet rings were replaced with sections of Platcover magnet rings with matching polarity. Second, the original flat or ribbon type anodes were replaced with narrower flat anodes and anodes with half-round cross sections to minimize the influence of the local field variations. (See figure 2-7.) Anode tests were conducted with flat anodes 5.6, 4.6, and 3.7 mm wide and half-round anodes 3.2 mm wide.

2.2.2 CATHODE SUBASSEMBLIES

Three different types of cathode baffles were tested. Two keeper potential baffle designs were tested as well as a cathode potential baffle. These were similar to the subassemblies performance tested in the 12 cm hexagonal thruster and used the same 3.2 mm diameter cathode with a 0.5 mm diameter orifice.

The keeper potential baffle cathode subassemblies had 1.25 cm diameter baffle support tubes with an annulus or solid disk baffle located 1.5 mm downstream of the tube end. The annulus-shaped baffle had a 9.0 mm diameter. Both were made from 0.75 mm thick tantalum that was cantilevered from the support tube on 0.25 mm wires and were located 7.0 mm from the cathode orifice. The keeper electrode in both cases was a ring of 1.0 mm diameter tantalum wire suspended on spotwelded wire 1.3 mm from the cathode as shown in figure 2-8.

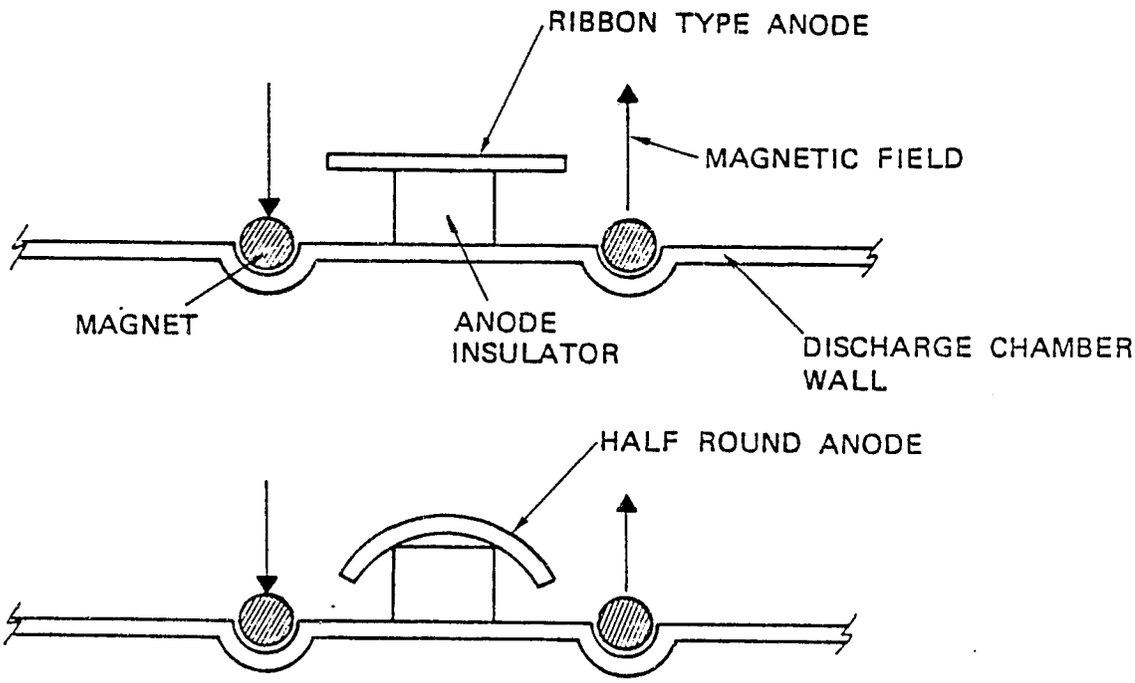

64815

Figure 2-7. Cutaway Schematic of the Hemispherical Thruster Anode Configurations

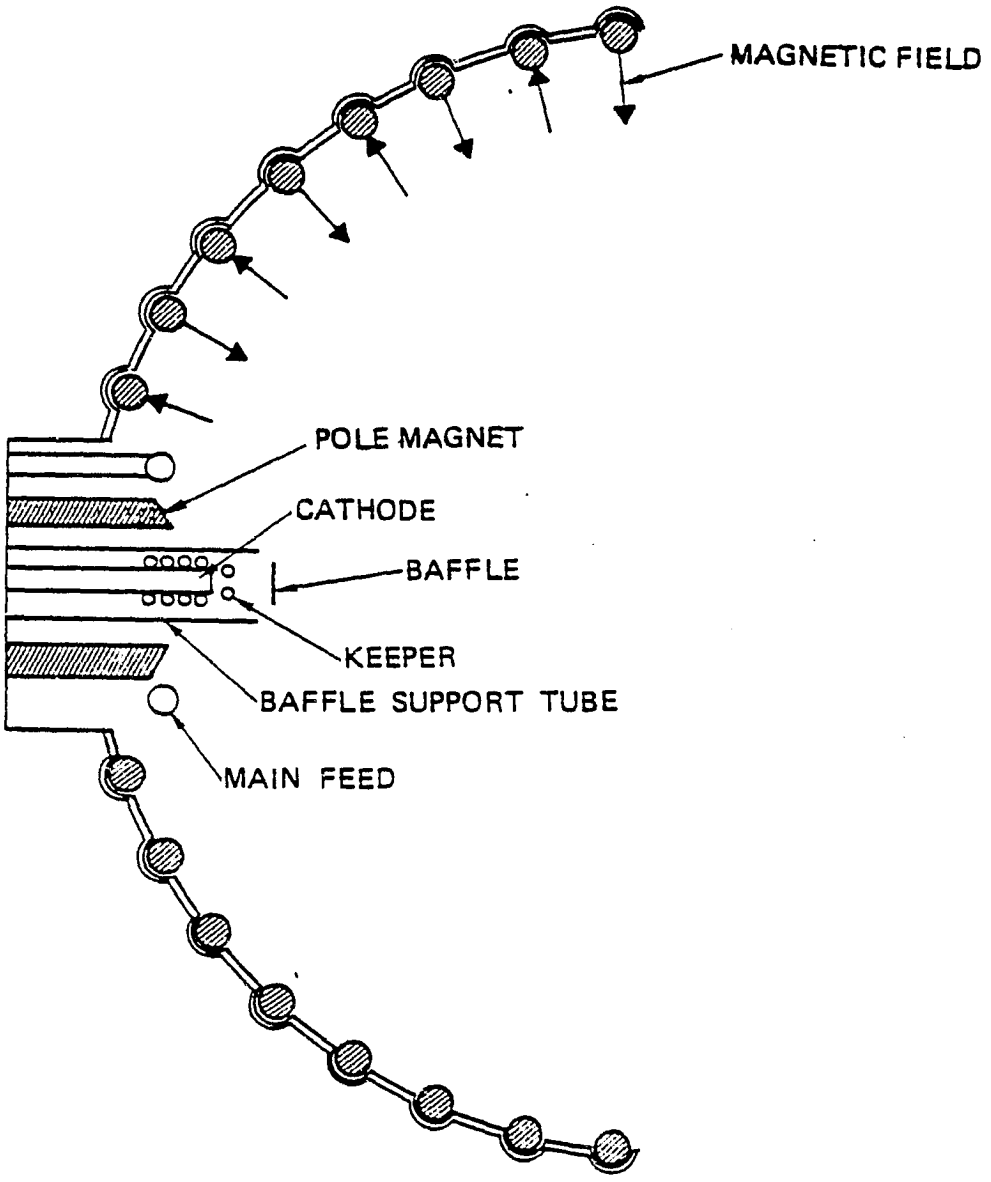

Figure 2-8. Cutaway Schematic of 11.8 cm Hemispherical Discharge Chamber with Keeper Potential Baffle

64818

The cathode potential subassembly was two concentric tubes around the 3.2 mm diameter cathode. A 1.1 cm diameter tube and spotwelded wires were supported by a 3.2 mm diameter tantalum keeper ring 1.5 mm downstream of the cathode orifice plate. An outer tube 1.5 cm diameter and spotwelded wires supported the 1.1 cm diameter disk 1.5 mm downstream of the tube end. The baffle operated at cathode potential.

2.2.3 ION OPTICS

The hemi thruster extraction grids were similar to those used on the hex thruster except they contained 10 percent fewer holes because the circular thruster shell rounded off the corners of the hexagonal array. Two-grid SHAG design ion optics were used consisting of a 69 percent geometric transparent screen and 22 percent transparent accel in an uncompensated pattern. The hole diameters were 1.2 and 2.2 mm in the screen and accel, respectively. The grids were fabricated from 0.25 mm thick molybdenum that had been hydroformed into a 4.0 mm deep dish for thermal stability. The grids were separated with 1.0 mm thick boron nitride washers spaced at 4.2 cm intervals around the perimeter.

2.2.4 GROUND SCREEN-NEUTRALIZER ASSEMBLY

The same 65 cm diameter stainless steel ground screen and neutralizer assembly described in the hex thruster test apparatus was used for the hemi thruster test. The tantalum filament was slightly farther from the edge of the ion beam as the beam diameter was reduced an average of 1.0 cm due to fitting the hex hole array to the circular discharge chamber cross section.

2.3 POWER CONDITIONING

The power conditioning was a dc-dc inverted flight prototype breadboard designed and built on a previous program to operate at 0.5 ampere and 1200 volts. The inverter drive was increased to uprate the output to 0.9 ampere at 1200 volts during the previous MESC discharge chamber inert gas program. Further output increases were limited by the magnetics used in the circuit.

A higher power laboratory supply was integrated into the existing power conditioning to increase beam supply capability. Tests found the laboratory supply output ripple was too great to permit stable thruster operation. The laboratory supply ripple was 600 volts peak-to-peak compared to a breadboard ripple of 90 volts under similar operating conditions. Subsequent testing was limited to the 0.9 ampere of the breadboard supply.

2.4 BEAM AND DISCHARGE PROBES

2.4.1 FARADAY BEAM PROBE

Three Faraday cup type probes were used to measure the ion beam distribution by traversing through the beam plasma at right angles on the thruster centerline at the locations shown in figure 2-9. Two probes crossed the beam axis 22 cm downstream of the accel grid. One of these was a slit probe and the other was a cylindrical probe.

The slit probe was used to measure beamspread and to confirm the cylindrical probe was collecting the entire beam width. The slit probe was a concentric tube assembly with a 1.27 cm diameter internal tube used as the probe collector. Electrical isolation between the tubes was accomplished by short teflon sleeves on the ends of the internal tube.

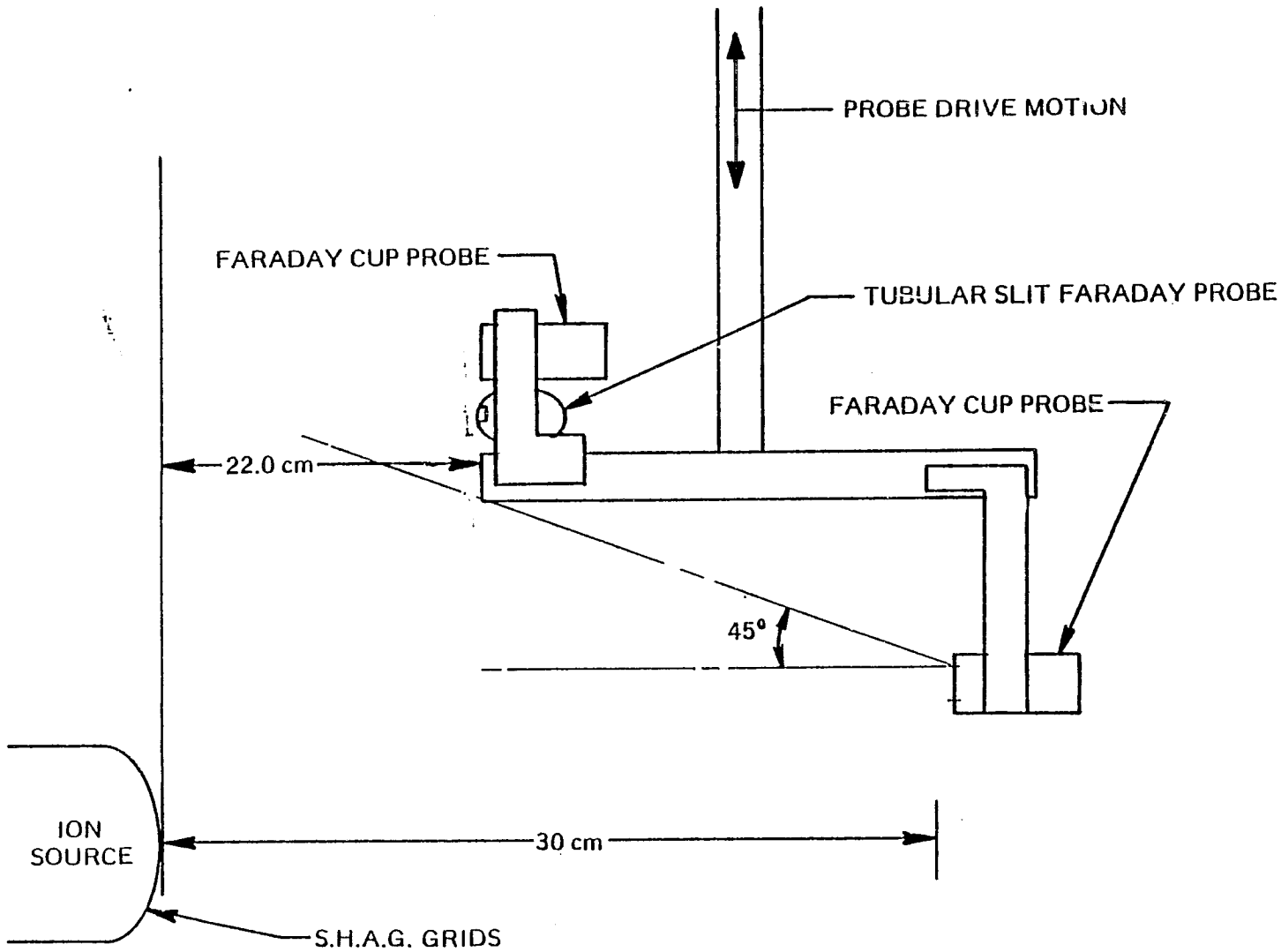

Figure 2-9 Relative Position of the Faraday Probes in the Ion Beam

The collector tube had a 25.5 x 0.64 cm opening that was aligned with the opening in the outer tube. The tubes had wall thicknesses of 0.38 mm.

A cylindrical probe located 30 cm downstream of the accel grid (see figure 2-9) was identical to the one at the 22 cm location. Each Faraday cup orifice was 1.27 diameter.

During operation, the probe collectors were biased negative with respect to ground to minimize electron collection. No electron suppression grids were used on the probes. Data from the probes were recorded on an x-y plotter with the x-axis indicating probe drive position and the y-axis recording the current collected by measuring the potential across a 300 ohm resistor.

2.4.2 LANGMUIR DISCHARGE PROBE

A 2.0 mm by 0.46 mm diameter sheathed heater type Langmuir probe was used to measure discharge chamber plasma characteristics of the hex thruster.[1] The probe was attached to a vacuum bulkhead control rod for positioning. Rod motion located the probe 1.0 to 4.5 cm from the discharge chamber center line in the plane of boundary anodes 2 through 5. A schematic numbering the boundary anodes is shown in figure 2-10.

The Langmuir probe potential was controlled by a 100V dc power supply electrically "floating" at high voltage. An x-y plotter, also at high voltage, recorded probe potential and current during data taking. Data were recorded at potentials negative and positive with respect to cathode common by changing the supply polarity and rapidly varying its output to produce a continuous current-voltage plot. Probe floating potential was recorded at each location for which a plot was made by switching the supply out of the probe circuit. A transformer in

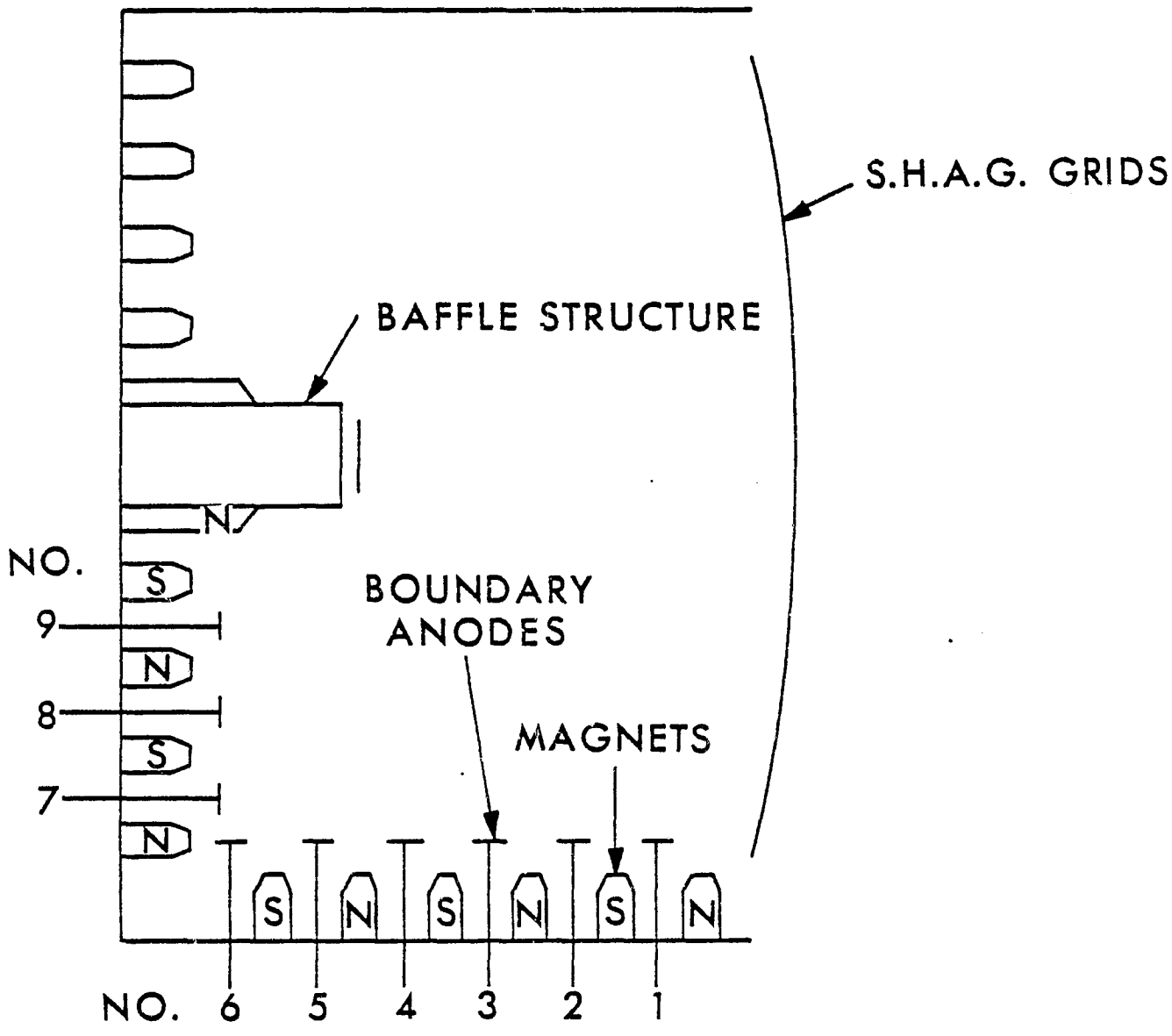

Figure 2-10. Cutaway Schematic 12 cm MESC Discharge Chamber Showing Anode Number Sequence

60986

the supply and plotter ac lines electrically isolated both from ground while data were being recorded. A 6 pole switch disconnected the high voltage leads from the supply and plotter when not in use. The probe was allowed to float when it was not being used to minimize any possible disturbance to thruster operation.

2.4.3 E x B PROBE DRIVE

An E x B probe drive was designed and fabricated to be used to investigate the radial distribution of single and double charged ions in the exhaust plasma of MESC thrusters. The probe itself was supplied GFE from NASA Lewis Research Center, Cleveland, Ohio, and the probe drive mechanism was designed and built at XEOS.

Accurate data collection imposes several stringent requirements on the probe and its controlling drive mechanism. Good radial resolution can be realized by using a highly collimated probe to collect ion current from selected points on the accel grid. However, collimation introduces an error in the current collected because of the beam space charge divergence. To overcome this problem, it is essential to monitor the ion current from a grid point at several different angles. Assuming symmetry, the probe angle need only be changed in one plane.

The probe drive was designed to keep the probe aimed at one point on the accel while measuring the ion current collected at ± 12 degrees to the thruster axis. Angular movement of the probe was accomplished by the differential motion of the two control tubes attached to the body of the probe as shown in figure 2-11.

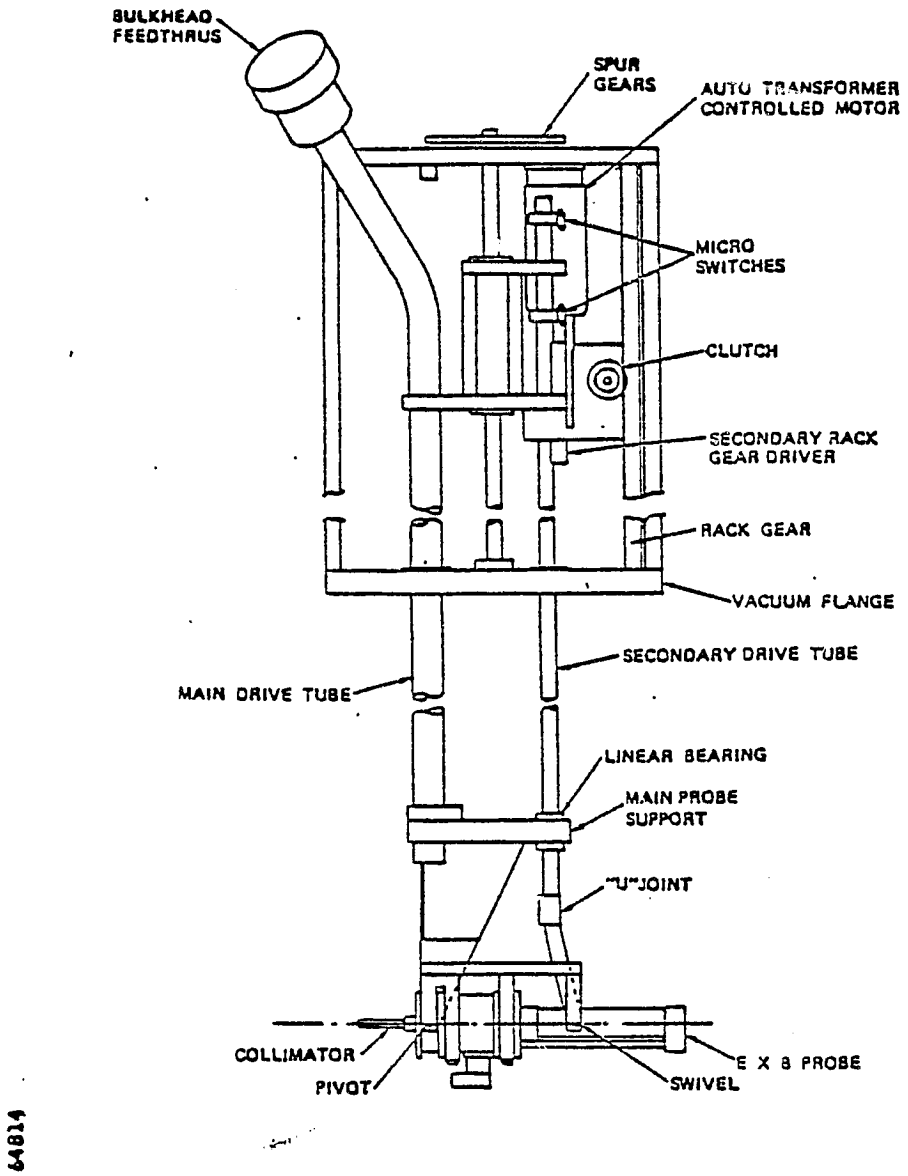

Figure 2-11. Schematic of E x B Probe Drive Mechanism

The main shaft and secondary rod were locked together until the probe reached the desired position in the exhaust plasma. The electromechanical lock was then removed and the drive clutch engaged. Main tube movement produced secondary rod motion by rotating the clutch pinion gear along the rack gear attached to the probe drive support structure. By selecting the appropriate gear ratio of the clutch pinion and support rack gear and drive pinion and secondary rod rack gear, the probe collimator aimed at a point on the accel grid. Microswitches limited probe angular deflection to prevent gear runoff.

The pointing error caused by gear backlash and angular runout due to the linear approximation of circular motion totaled about 1.2 degrees. The probe collimator had a 4.5 degree resolution or 3.5 times greater than the possible error.

The E x B probe control circuit diagram is shown in figure 2-12. Signals from a ten-turn potentiometer attached to the secondary pinion and the nanoampere meter in series with the collector were fed into an x-y plotter to display ion current as a function of probe angle. The nanoampere meter, H-P 425, had a 70K ohm output impedance with a 0 to 5 volt signal to the plotter. Probe radial position in the beam was determined from another ten-turn potentiometer coupled to the main probe drive. The main drive position was read from a calibrated panel meter. Batteries were used to bias the collector guard ring and deflection plates within the probe to minimize the collector signal noise. The batteries had output voltage from 0 to 100 volts and were electrically tied to the vacuum system-power conditioner ground. The potential applied to the plates or the guard ring was monitored with calibrated panel meters as shown in the circuit schematic depicted in figure 2-12.

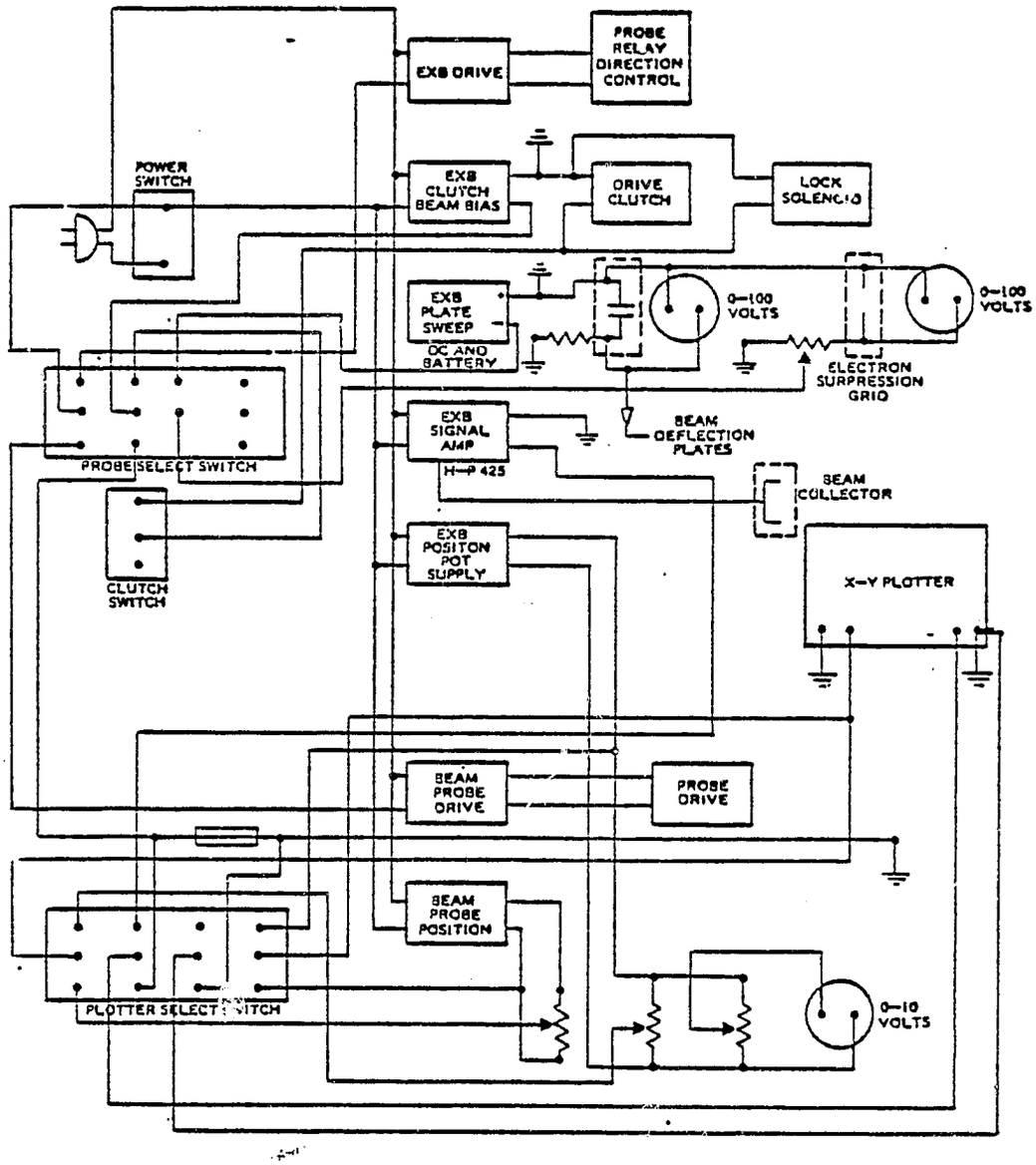

Figure 2-12. Probe Control Circuit Diagram

2.4.4 GAS FLOW MEASUREMENTS AND CONTROLS

Gas flows through the thruster cathode and main feed were controlled and measured with the same apparatus used in the previous program.[1] The flow to the cathode and main were regulated with two needle valves. Rough measurements of gas flow rates were made with rotometers in series with the valves and the mass flow transducer data were used to calculate performance.

SECTION 3

TEST RESULTS

3.1 HEXAGONAL THRUSTER TESTS

Two types of tests were conducted with the 12 cm hex thruster in this phase of the program. The first set of tests established baseline performance data of the optimized hex thruster argon and xenon operation. The second set determined the performance impact of cathode design changes on baseline hex thruster performance. A comparison between sets of data permitted selection of the cathode design used in the 12 cm hemispherical thruster argon and xenon tests.

3.1.1 BASELINE THRUSTER TESTS

The 12 cm hex thruster was operated in several different gas flow patterns during the baseline and subsequent tests to determine the thruster performance over the widest possible range of operating conditions. Single gas operation used the same gas in both the cathode and main feed circuits. Dual gas, or mixed mode, used different gases in the two circuits. The flow ratios between the cathode and main feed were adjusted to give optimum performance. The test results were corrected for neutral gas backflow from the vacuum system into the discharge chamber and the double charged ion current in the beam.[1] In the case where different gases were flowing through the cathode and main feed, "mixed mode," the double charged ion correction was calculated by assuming the test operating conditions produced a percentage of double charged ions proportional to the flow. These were summed to find the total double charged beam current as shown in Appendix A.

The neutral backflow from the vacuum system into the discharge region was calculated[1] from partial pressures of the gases recorded during the tests.

The performance of the hex thruster under various modes of operation is shown in figure 3-1. Argon performance of 79 percent mass utilization efficiency at 303 eV/ion was obtained in the optimized configuration. Xenon performance of 90 and 96 percent mass utilization was achieved at 225 and 356 eV/ion, respectively.

Dual gas, or mixed mode, hex thruster performance was found to resemble the single gas operational characteristics of the gas flowing through the main feed. For example, tests conducted with argon main gas flow achieved 51 to 79 percent ionic mass utilization at 234 to 425 eV/ion. Xenon main gas flow tests produced 74 to 92 percent ionic mass efficiency at 180 to 220 eV/ion. Comparing these results with the single gas test results shows the argon main flow performance was slightly worse than single argon gas, while the xenon main flow performance was slightly better.

In order to correlate the results from mixed mode and single gas tests, generalized mass utilization efficiency as well as ionic mass utilization efficiency was calculated. Ionic mass utilization efficiency is the ratio of the total equivalent single charged ion beam current to the total mass flow amp equivalent. Generalized mass utilization efficiency, or distribution efficiency, is the equivalent single gas mass utilization efficiency that should be used to compare the power-to-thrust ratio performance of mixed mode and single gas thruster operation.[11] Generalized mass utilization efficiency is the product of ionic mass efficiency and a distribution relationship derived in Appendix B. The distribution relationship is:

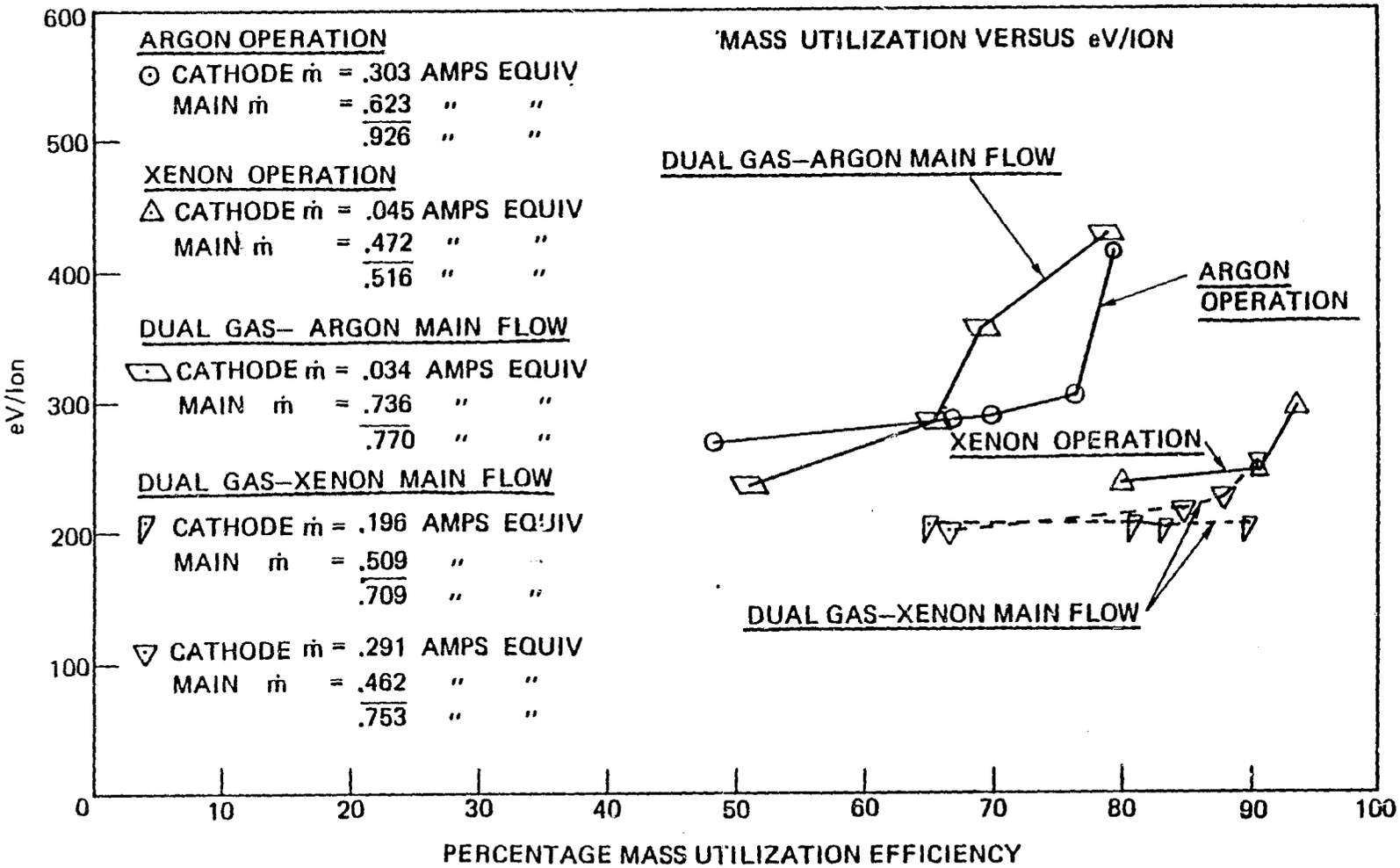

Figure 3-1. Hexagonal Thruster Optimum Performance Curve

$$\eta_d = \frac{\left[f_1 \left(\frac{q}{m}\right)_1^{1/2} + f_2 \left(\frac{q}{m}\right)_2^{1/2} \right]^2}{f_1 \left(\frac{q}{m}\right)_1 + f_2 \left(\frac{q}{m}\right)_2} \qquad (6)$$

where f is the mass flow fraction and (q/m) is the charge-to-mass ratio of the gases.

Although xenon main flow mixed mode eV/ion performance looked good, it was less efficient than single xenon gas. Using the distribution relationship, the above xenon main flow dual gas tests produced thrust equivalent to single gas xenon mass utilization of 68.5 and 85.1 percent.

3.1.2 2.3 CM CATHODE MAGNET TESTS

Tests with the original 2.3 cm hex thruster cathode magnet were conducted with the two sizes of single tube keeper potential support subassemblies described previously in the Apparatus Section of this report. The signal tube supported both the keeper electrode and the baffle and extended into the main discharge plasma.

Two types of baffles were tested with the single diameter support tube. The first type, a 1.1 cm diameter solid baffle disk, produced poor mass utilization at increased discharge energy consumption in a relative unstable discharge. Test results of the solid disk produced 69 percent argon mass efficiency at 423 eV/ion and 86 percent xenon mass efficiency at 270 eV/ion. Dual gas operation with xenon main flow produced 70 percent utilization at 311 eV/ion. Anode operating potentials during these different mode tests were 52, 39, and 40 volts, respectively.

Changing to the second type of baffle, a 1.3 x 0.8 cm annulus, improved thruster performance and operational stability. The annular baffle tests achieved 82 percent xenon mass utilization at 260 eV/ion in a 29 volt discharge and 68 percent argon mass efficiency at 309 eV/ion in a 42 volt discharge with nominal cathode-main feed flow rates. Reducing the cathode xenon gas flow rate to $\sim$ 0.020 ampere equivalent, about 1/2 nominal, produced 35 to 39 volt discharge operation. Dual gas operation with xenon main flow achieved 80 percent ionic mass efficiency at 230 eV/ion in a 38 volt discharge.

Comparing the xenon performance of the baseline and small tube, annular baffle cathode subassemblies found the change increased discharge energy consumption 33 percent but reduced the single gas anode operating potential 8 to 10 volts. Reduction in anode operating potential could be used to reduce sputtering and extend thruster lifetime during a long-term mission. Time was not available to optimize performance by changing the baffle structure axial position in the discharge chamber or adjusting the boundary anodes to produce a more desirable current density distribution.

The large downstream diameter baffle support tube was tested with an annular baffle 1.5 x 0.47 cm diameter. The results of these tests looked similar to those produced with the single diameter support tube-annular baffle tests. Argon mass utilization efficiency of 68 percent at 300 eV/ion and xenon mass efficiency of 91 percent at 236 eV/ion were achieved. Dual gas operation with xenon main flow produced 82 percent ionic mass efficiency at 278 eV/ion. During xenon operation, anode potential was 30 volts and appeared similar to the operation found in the single diameter tube annular baffle tests. Figure 3-2 is a graph of the thruster performance seen with the indicated 2.3 cm magnet-baffle assembly. Optimum baseline baffle-magnet test results have been plotted on the same graph for comparison.

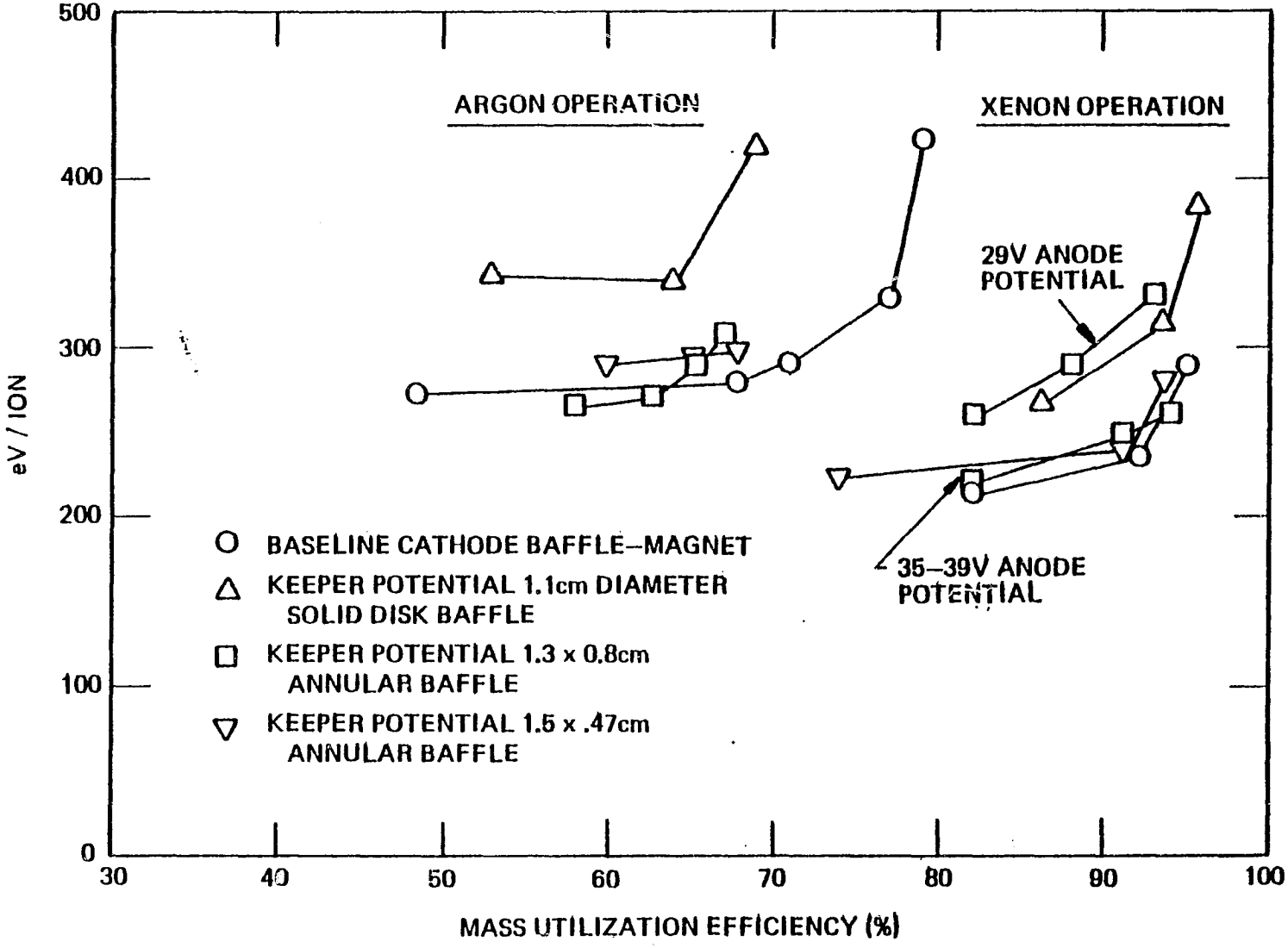

Figure 3-2. 2.3 cm Cathode Pole Magnet Hex Thruster Performance Comparison with Different Baffle Design

3.1.3 3.3 CM CATHODE MAGNET TESTS

Tests with the larger, 3.3 cm cathode magnet were conducted with an annular baffle. Separate support tubes were used to position the baffle and keeper relative to the cathode. The 1.1 cm inner tube supported the keeper ring and operated at keeper potential. The 1.9 cm outer tube supported the 1.5 x 0.47 cm annular baffle and was electrically isolated from the keeper and adjacent hardware (see Figure 2-5). Thus, the potential of the outer tube-baffle could be selected during the course of a test by a change in the esternal wiring.

Single gas test results showed changing to a larger cathode magnet-baffle reduced thruster performance. The hex thruster achieved 68 percent argon mass efficiency at 344 eV/ion and 91 percent xenon mass efficiency at 319 eV/ion in a 36 volt discharge. Better argon performance was achieved with a cathode potential baffle. Tests conducted with the baffle electrically "floating" had the same performance and operation characteristics as the keeper potential baffle tests. The baffle floating potential was found to be equal to the keeper potential in all cases.

Dual gas tests with xenon main flow produced the best performance when using a cathode potential baffle. Ionic mass utilization efficiency of 80 percent was obtained at 224 eV/ion. This performance represents a 2 percent reduction in mass efficiency and a 16 percent reduction in eV/ion compared to the small tube-annular baffle performance.

A plot of the 3.3 cm cathode single gas performance is presented in Figure 3-3. Argon and xenon performance is plotted for the keeper and cathode potential baffle configuration and the baseline cathode configuration. It should be noted the "knee" of the xenon performance curve as well as the maximum mass efficiency shifts to slightly higher values when the baffle bias was changed from cathode to keeper potential.

3.1.4 CATHODE TEST EVALUATION

The performance of various cathode magnet and baffle configurations were evaluated in terms of plasma distribution, discharge potential, and discharge energy. The performance of the different configurations is grouped by operational gas flows in Tables 3-1, 3-2, and 3-3. The Relative Boundary Anode Current (last columns) was calculated by dividing through with the greatest anode current density recorded during that data point. The respective argon, xenon, and xenon main flow dual gas test data indicates changes to the cathode magnet-baffle impacted discharge plasma distribution as well as performance. Difference in plasma distribution can be inferred from changes in the relative anode current. Tests conducted with the various annular baffles had slight reductions in the relative current to the more upstream anode compared with the solid baffle tests. Thruster performance with the different magnet-baffles is shown in Figures 3-2 and 3-3.

A reduction in anode operating potential was seen when an annular baffle was substituted for the solid disk in the same thruster assembly. Solid disk anode operating potentials were typically 5 to 10 volts greater than produced by similar operating conditions with either annular baffle as can be seen in Tables 3-1 and 3-2. The reduction in anode potential produced a reduction in performance. As a reduction in anode potential

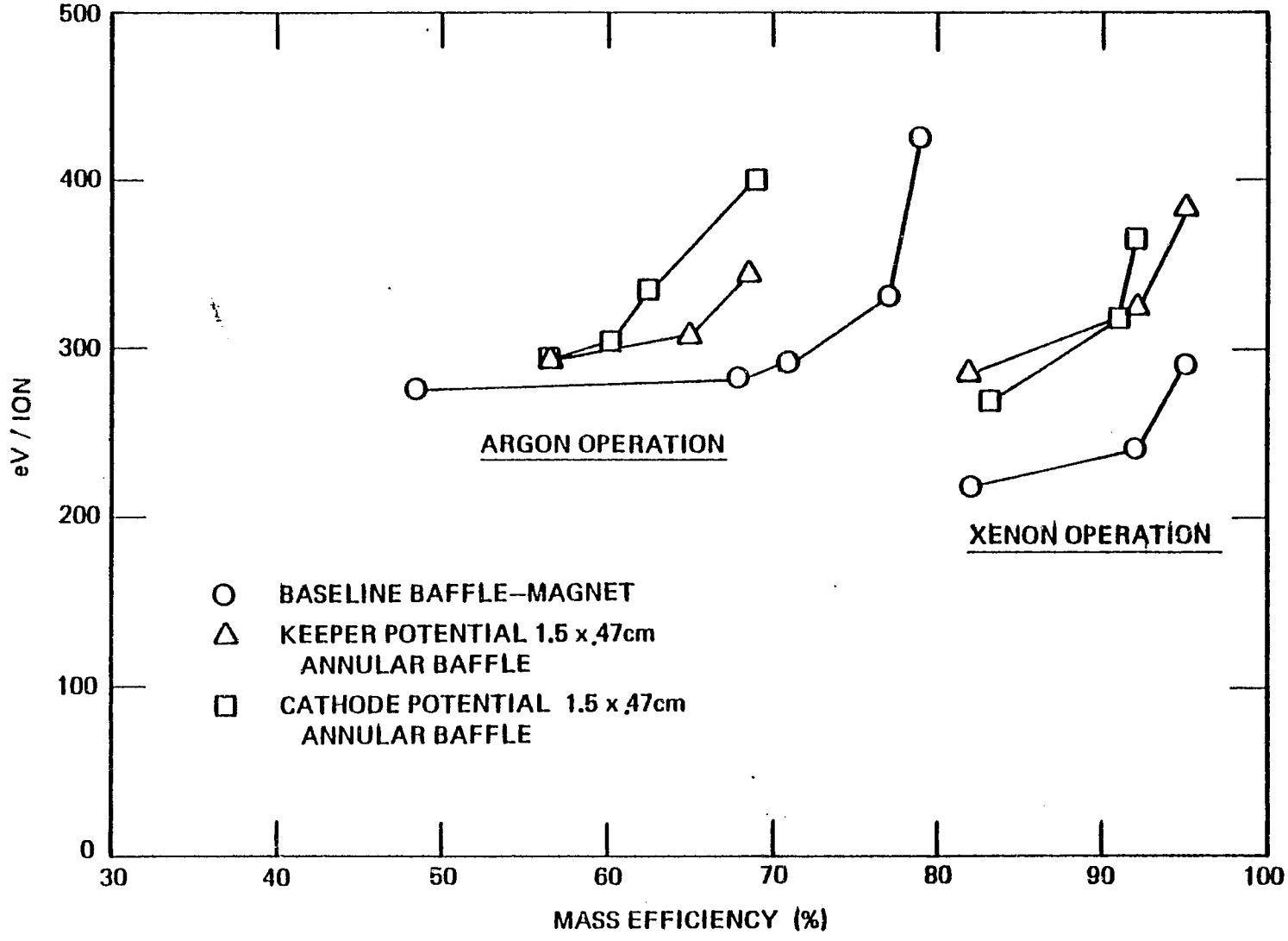

Figure 3-3. 3.3 cm Cathode Pole Magnet Hex Thruster Performance Comparison with Different Baffle Potentials

TABLE 3-1

HEXAGONAL THRUSTER ARGON PERFORMANCE WITH DIFFERENT BAFFLE CONFIGURATIONS

TEST CONFIGURATION	MAGNET DIAMETER (cm)	BAFFLE			ANODE POTENTIAL (volts)	TOTAL GAS FLOW (amp-equiv)	eV/ion	MASS EFFICIENCY (percent)	RELATIVE BOUNDARY ANODE CURRENT				
		TYPE	DIAMETER (cm)	POTENTIAL					Anode Number				
									1	2	3	4	5
BASELINE	2.3	dual tube	1.1 (solid)	cathode	52	.918	303	77	.54	1.0	.86	.37	.67
SMALL MAGNET	2.3	single tube	1.1 (solid)	keeper	49	.918	423	69 (unstable)	.70	1.0	.92	.52	.82
SMALL MAGNET	2.3	single tube	1.3 x .8 (annulus)	keeper	42	1.087	309	67	.71	1.0	.91	.45	.72
SMALL MAGNET	2.3	single tube	1.5 x .47 (annulus)	keeper	46	.941	300	68	.70	1.0	.97	.43	.80
LARGE MAGNET	3.3	dual tube	1.6 (solid)	keeper	50	1.013	344	68	.84	.81	1.0	.34	.65

TABLE 3-2

HEXAGONAL THRUSTER XENON PERFORMANCE WITH DIFFERENT BAFFLE CONFIGURATIONS

TEST CONFIGURATION	MAGNET DIAMETER (cm)	BAFFLE			ANODE POTENTIAL (volts)	TOTAL GAS FLOW (amp-equiv)	eV/ion	MASS EFFICIENCY (percent)	RELATIVE BOUNDARY ANODE CURRENT				
		TYPE	DIAMETER (cm)	POTENTIAL					Anode Number				
									1	2	3	4	5
BASELINE	2.3	dual tube	1.1 (solid)	cathode	40	.500	245	91	.58	.94	1.0	.58	.71
SMALL MAGNET	2.3	single tube	1.1 (solid)	keeper	40	.500	270	86	.46	.88	1.0	.60	.75
SMALL MAGNET	2.3	single tube	1.3 x .8 (annulus)	keeper	30	.525	221	82	.56	.85	1.0	.49	.74
SMALL MAGNET	2.3	single tube	1.5 x .47 (annulus)	keeper	32	.622	236	91	.53	.88	1.0	.57	.73
LARGE MAGNET	3.3	dual tube	1.5 x .47 (annulus)	cathode	36	.529	319	91	.89	.88	1.0	.33	.60

TABLE 3-3

HEXAGONAL THRUSTER DUAL GAS PERFORMANCE WITH DIFFERENT BABBLE CONFIGURATIONS

TEST CONFIGURATION	MAGNET DIAMETER (cm)	BAFFLE			ANODE POTENTIAL (volts)	TOTAL GAS FLOW (amp-equiv)	eV/ion	MASS EFFICIENCY (percent)	RELATIVE BOUNDARY ANODE CURRENT				
		TYPE	DIAMETER (cm)	POTENTIAL					Anode Number				
									1	2	3	4	5
BASELINE	2.3	dual tube	1.1 (solid)	cathode	42	.652	220	97.2	.46	.96	1.0	.62	.65
SMALL MAGNET	2.3	single tube	1.1 (solid)	keeper	40	.708	311	70.0 (unstable)					
SMALL MAGNET	2.3	single tube	1.3 x .8 (annulus)	keeper	39	.591	232	85.0	.62	1.0	1.0	.58	.74
SMALL MAGNET	2.3	single tube	1.5 x .47 (annulus)	keeper	37	.629	278	82.0	.54	.82	1.0	.31	.48
LARGE MAGNET	3.3	dual tube	1.5 x .47 (annulus)	cathode	46	.729	223	80.0	.74	.86	1.0	.40	.58

implies a reduction in discharge chamber ionic sputtering, the annular baffle design could be used to extend thruster lifetime in future long-term missions.

Xenon performance of the 3.3 cm magnet assembly was improved when the baffle potential was changed. Switching from cathode-to-keeper or float baffle potential shifted the high mass efficiency section of the xenon performance curve toward greater mass utilization as can be seen in Figure 3-3. The performance improvement seems to imply a reduction in the "fixed" discharge chamber losses resulted from the baffle potential switch.

The performance of the hex thruster was also effected by changes in the cathode magnet-baffle design. Thruster performance is expressed as how much discharge energy is needed to achieve a certain level of propellant mass utilization efficiency with a given thruster discharge chamber. For comparison purposes, it is necessary to consider both components of performance simultaneously. As performance is normally given as a set of curves plotting mass utilization as a function of eV/ion, it seems reasonable to use features of the performance curves for a numerical comparison of operation. The discontinuity in slope or "knee" between low and high mass utilization operation of the thruster is typical of most performance plots and a convenient feature for reference.

A numerical comparison of baseline and cathode magnet-baffle test configuration is calculated from test results and presented in Table 3-4. The eV/ion ratio listed in the column under that heading is defined as the ratio of eV/ion values of the test configuration and the baseline configuration taken from the knees of their respective performance curves.

TABLE 3-4

CATHODE PERFORMANCE COMPARISON CHART

PERFORMANCE COMPARISON WITH BASELINE CATHODE DESIGN

MAGNET DIA. (cm)	BAFFLE TUBE DIA. (cm)	BAFFLE TUBE TYPE	BAFFLE CONFIGURATION	ARGON eV/Ion* Ratio	ARGON PI	XENON eV/Ion* Ratio	XENON PI**	XENON MAIN FLOW MIXED MODE eV/Ion* Ratio	XENON MAIN FLOW MIXED MODE PI**
2.3	1.3	single	solid	1.57	-0.33	1.19	-0.16	1.73	-0.41
2.3	1.3	single	annulus (1.3 x 0.8 cm)	1.10	-0.14	.96	-0.08	1.05	-0.12
2.3	1.9 (end)	single	annulus (1.5 x 0.47 cm)	1.07	-0.10	1.05	-0.047	1.16	-0.25
3.3	1.9	double	annulus (1.5 x 0.47 cm)	1.27	-0.21	1.32	-0.23	1.09	-0.15

*eV/ion ratio between test cathode indicated and baseline

**Performance impact: Defined as $1 - (\text{eV/ion}_B/\text{mass eff}_B)/(\text{eV/ion}_I/\text{mass eff})$

where B and I indicate baseline and test cathode listed at left

The "Performance Impact Parameter" tabulated in Table 3-4 under the column heading, PI, is defined as

$$\text{Performance Impact} = 1 - \frac{\dfrac{\text{eV/ion}_B}{\text{Mass Eff}_B}}{\dfrac{\text{eV/ion}_I}{\text{Mass Eff}_I}} \qquad (7)$$

where eV/ion_B and eV/ion_I and mass eff_B and mass eff_I were the eV/ion and mass utilization efficiencies knees of the baseline and test cathode respective performance curves. The ratio term was subtracted from unity in order to associate a negative number with loss of performance. This calculation is a linear extrapolation indicating the percentage performance loss in substituting the test cathode configuration for the baseline. However, the comparison did not take into consideration the possibility of discharge chamber reoptimization, differences in discharge chamber erosion rates, differences in beam spread, etc. The table simply indicates the performance changes produced by making these changes to the cathode magnet-baffle of a fixed MESC discharge chamber. A negative P.I. value indicates an adverse impact on performance.

The tabulated values indicated there was a performance loss associated with all four cathode magnet-baffle tests configurations. For single gas operation, the minimum impact on performance was seen with the 2.3 magnet and a single baffle tube with different upstream and downstream diameters operating at keeper potential with a 1.5 x 0.47 cm annular baffle. By contrast, minimum performance impact on xenon main flow dual gas operation was produced with the 2.3 cm magnet and a single diameter keeper potential tube with a 1.3 x 0.8 cm annular baffle.

3.2 HEMISPHERICAL THRUSTER TESTS

Hemi thruster tests were conducted with three different types of cathode magnet-baffle designs. These designs were selected from those tested in the hex thruster cathode tests. They included a scaled-down baseline design and a keeper potential single tube with an annular baffle. A keeper potential solid disk was included to determine how it would effect hemi thruster performance. The three cathode magnet-baffle designs were tested with several anode designs and several anode-to-magnet placements.

3.2.1 PERIPHERAL MAGNETIC FIELD-ANODE PLACEMENT

Anode design changes were prompted by the low flux density, nonuniform peripheral magnetic field in the hemi discharge chamber. The electron diffusion current flow to the anodes is inversely proportional to the magnetic field across the anode parallel to the discharge chamber walls. Adjusting the anodes for inert gas operation relocated them closer to the walls of the discharge chamber. However, the closer the anodes were brought to the walls, the greater were the point-to-point differences in the anode magnetic field. These differences in the peripheral magnetic field concentrated the electron current at points of minimum field along the anode rings. Eventually, attempts to minimize diffusion current by moving the anodes closer to the magnets concentrated the electron current at two points and melted the stainless steel anodes.

Different anodes were tested to see how they effected magnetic field uniformity and inert gas plasma operation. Tests were conducted with ribbon anode widths of 5.5, 4.5, and 3.8 mm and half round anodes of 3.2 mm diameter. Setting the anodes a uniform radial distance from the magnet pole surface (MPS) produced wide differences in the peripheral field. For example, the half round anodes 3.0 mm from the MPS had an average field of 8.6 millitesla with a maximum and minimum of 13.5 and

and 4.0 millitesla, respectively. Argon-xenon single gas tests conducted with the above configuration produced localized melts in the anode sections at the two points of minimum field.

3.2.2 HEMI THRUSTER OPERATIONAL TESTS

Hemi thruster inert gas operational tests were conducted with two types of anode placements: the anodes set a uniform distance from the MPS or the anodes located varying distances from the MPS in order to match point-to-point variations in the local magnetic field. Tests with the first type of anode placement produced large apparent variation in the electron current density to different sections of the same anode and high discharge energy consumption performance. Test results with the second anode placement showed a reduction in the point-to-point differences in the electron current distribution and improved thruster eV/ion versus mass efficiency performance.

The best argon performance was obtained using half round anodes located varying distances from the MPS and a keeper potential annular baffle. Argon mass efficiencies of 40 to 67 percent were achieved at 270 to 428 eV/ion, respectively.

Conversely, the best xenon performance was achieved with the same half round anode placement but using the cathode potential, dual tube magnet-baffle structure with a 1.1 cm solid disk. This configuration achieved 79 to 90 percent xenon mass utilization at 270 to 389 eV/ion. Substituting the single keeper potential baffle support tube with an annular baffle increased power consumption to 300 and 425 eV/ion for similar mass efficiencies.

The number of tests conducted in mixed mode was insufficient to determine which cathode magnet-baffle and anode configuration produced the best xenon main flow, dual gas operation. However, dual gas tests conducted with 4.5 mm wide ribbon anodes located varying distances from the MPS with a keeper potential annular baffle produced 71 to 79 percent ionic mass efficiency at 307 and 387 eV/ion, respectively.

3.2.3 HEMI PERFORMANCE EVALUATION

A study of the test data was undertaken to reconcile the apparent differences between hex and hemi thruster inert gas performance. Hemi thruster inert gas performance showed greater eV/ion and lower attainable argon mass utilization than hex thruster operation. This reduction in performance was attributable to several causes. The most likely causes were reduction in neutral molecule residence time and an increase in the ion recombination due to a weaker, nonuniform magnetic field. The latter resulted from increases in the hybrid radius losses associated with the lower magnetic flux density.

3.2.3.1 Neutral Residence Time

Changing from the hex to hemi thruster configuration effectively reduced the discharge chamber length from 8.8 to 5.7 cm. Shortening the chamber reduced both ionic recombination wall area and the neutral molecule residence time in the discharge region. If the conditions in the discharge plasma were such that the mean-free ionization path were greater than the 5.7 cm chamber length, ionization probability would as it has 1/3 the atomic mass, 1.7 the thermal velocity, and 1/2 the ionization cross section of xenon. The mean-free ionization path was calculated for argon and xenon using the relationship developed by Masek[12] assuming uniform distribution of electrons and neutrals in the discharge region. The masek relationship is:

$$\lambda = \frac{v_n}{n_m \Sigma_m + n_p \Sigma_p} \qquad (8)$$

where:

v_n = thermal velocity of the neutrals

n_m, n_p = densities of Maxwellian electrons and primary electrons, respectively

Σ_m, Σ_p = product of velocity and the ionization cross section of the Maxwellian and primary electron at the respective energy levels.

Argon and xenon were found to have mean-free-ionization-paths of 5.7 and 2.2 cm, respectively. The argon mean path approximately equaled the hemi discharge chamber length.

3.2.3.2 Hybrid Radius Losses

The nonuniform, low flux density peripheral magnetic field increased the hybrid recombination losses and was another source of discharge inefficiency in hemi thruster inert gas operation. Xenon test data indicated the best performance was achieved when the boundary anodes were located in a uniform field which was less than the maximum possible for stable operation. Uniform anode magnetic field was produced by varying the displacement between the MPS and sections of individual anodes.

Discharge operational stability was evaluated with a technique first used by Kaufman.[4] Sections of the anode array were disconnected from the discharge dc supply and allowed to electrically "float" in the discharge plasma. Tests with a relatively uniform 10.0 millitesla anode field showed no change in stability or plasma impedance until the anode area had been reduced more than 40 percent using the Kaufman technique. These results implied the 10.0 millitesla anode position

was a stable operating configuration. However, the 10.0 millitesla anode configuration did not produce better overall performance than the 8.0 millitesla anode configuration as expected from the Bohm diffusion considerations.[1]

Dividing thruster performance at the knee of the performance curve for discussion, the 8.0 millitesla anode configuration produced better performance above the knee than the 10.0 millitesla configuration. Conversely, the 10.0 millitesla configuration produced better performance below the knee. The 10.0 millitesla average magnetic field positioned the 4.5 mm wide anode an average of 1.3 mm from the MPS and produced 77 to 92 percent xenon mass efficiency (η) at 312 to 460 eV/ion. Substituting 3.2 mm half-round anodes in the same radial location produced 77 to 85 percent xenon η at 280 to 470 eV/ion at the same mass flow rates. Relocating the half round anodes farther from the MPS, in an 8.0 millitesla average field, at an average distance of 3.0 mm from the MPS produced 73 to 92 percent xenon η at 290 and 500 eV/ion, respectively. Several tests with different geometries produced similar results, namely, positioning the anodes closer to the MPS improved thruster performance until the average anode-magnet displacement was less than 3.0 mm. Anode positions closer than 3.0 mm continued to improve thruster performance at lower η but restricted the ultimate η.

This effect can be clearly seen in Figure 3-4, which is a graph of hemi thruster xenon performance using similar cathode and main mass flow rates but different anode geometries. The figure shows the wide anodes, farther from the MPS, produced greater corrected mass utilization efficiency than either half-round anode configuration. Also, the half-round (H-R) anodes located farther from the MPS, produced greater ultimate mass utilizations than the closer positions.

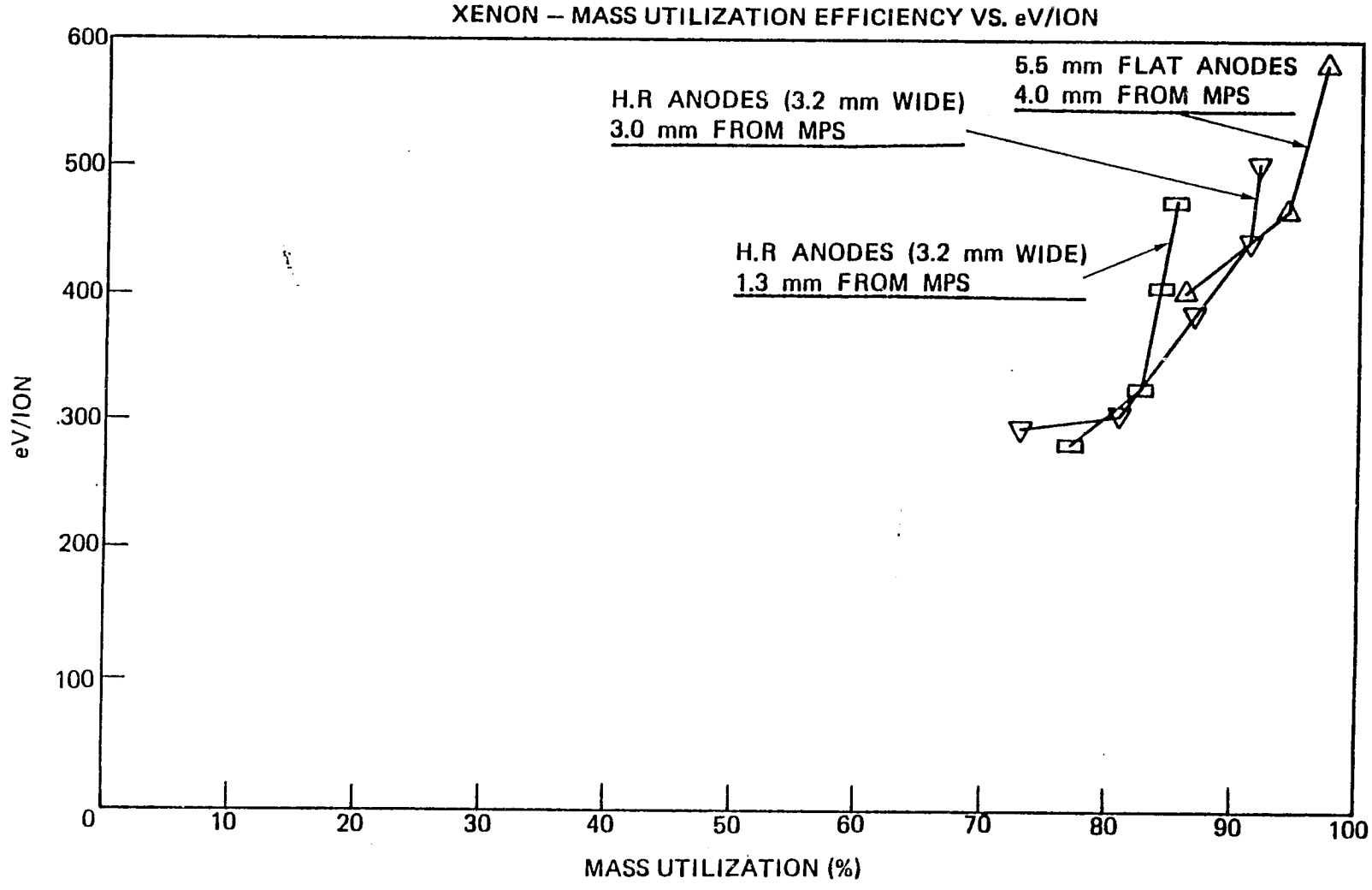

Figure 3-4. Comparison of Hemi Thruster Xenon Performance with Different Boundary Anodes Geometries

Conversely, the close and narrow anode geometries had lower eV/ion during low mass utilization operation as knee of the performance curves moved toward lower η's as the anodes were narrowed or positioned closer to the MPS.

These changes in thruster performance as a function of anode position apparently resulted from increased ionic recombination losses. Thruster discharge chamber performance is principally a function of two loss mechanisms: electron diffusion to the anodes and ion recombination losses on the walls and screen grid. From the Bohm diffusion relationship given previously, it can be seen a weak peripheral magnetic field produces rapid electron diffusion to the anodes and minimizes electron ionization probability which increases discharge energy consumption per ion generated (eV/ion). Conversely, a larger magnetic field increases the electron diffusion path and the electron ionization probability and reduces discharge eV/ion. The xenon test results showed an increase in anode magnetic field greater than an average of 8.0 millitesla increased discharge eV/ion at thruster mass efficiency operation above the performance curve knee. Hence, the gains in electron diffusion coefficient were offset by increases in discharge chamber losses at high mass efficiency operation.

Ionic wall recombination losses are governed by the magnetic flux density at the magnets and the anode-magnet geometry. The flux density sets the ionic hybrid radius (see Eqs. 4 and 5) while the anode-magnet geometry defines the ion wall recombination boundary. The wall recombination area is the magnet area exposed to the discharge plasma. This area is the product of the magnet "width," increased by the hybrid radius and the total magnet length of the discharge chamber. Magnet width in this case is defined as that portion of the magnet, toward the plasma, between the field lines from the magnet to the edge of the adjacent anodes. Hence, the wall

area exposed to the plasma increases as the anodes are positioned closer to the MPS, as shown in figure 3-5, at large magnet-anode edge angles, the gain in electron efficiency produced by stronger magnetic fields close to the magnets is dominated by the increases in recombination surface area. Increasing the ionic losses restricts the easily achievable mass utilization efficiency to lower values. High mass utilization can be achieved by reionizing an increased percentage of recombined ions. Increased ion losses can be inferred from the shift in the performance curve knee.

In order to determine the casual relationship between anode placement and recombination losses, it was necessary to know how many electrons were needed to produce a beam ion. The number of electrons per beam ion can be expressed as:

$$\text{Electron Efficiency} = \frac{I_D - I_B}{I_B} \qquad (9)$$

where I_D is the discharge current and I_B the uncorrected beam current. The uncorrected beam current is the positive high voltage supply current less the absolute value to the negative high voltage supply.

The impact of anode geometry change on performance can be seen in Tables 3-5 and 3-6 where a comparative study of the data collected with the hemi thruster is presented. The column headings indicate the calculated operational parameters arranged according to the average anode distance from the MPS. The "Anode Type" column lists the anode configurations being compared across the row. The potential difference between the anode and keeper electrode is approximately the primary electron energy. The "Electron Current Per Ion Beam"

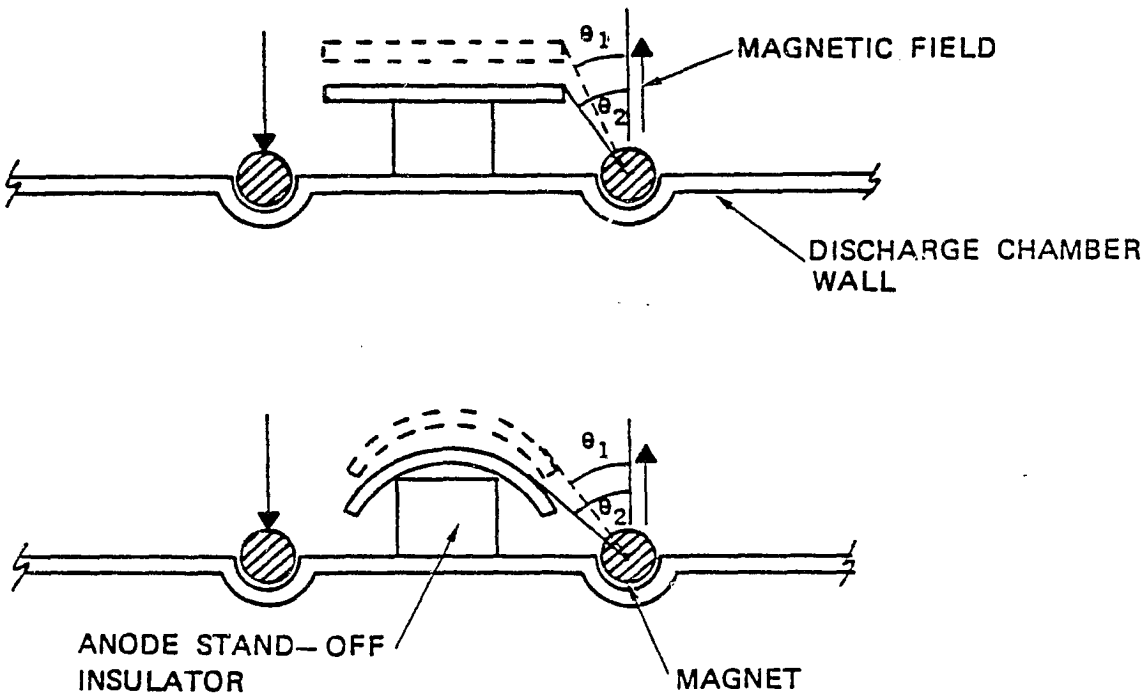

Figure 3-5. Cutaway Schematic of Hemispherical Thruster Anode Placement

64816

TABLE 3-5

XENON ELECTRON EFFICIENCY

Anode Type	Spacing to Magnet Pole Surface (mm)	Potential Difference Between Keeper and Main Discharge (volts)	Electron Current per Ion Beam Ratio	Total Mass Flow (amps equiv)	Main Discharge Current (amps)	Baffle Potential	Change in Exposed Wall Area	Corrected Electron Current per Ion Beam
4.5	2.5	26.0	7.42	.453	3.4	Keeper	.88	.99
H.R.	2.5		6.81	.490	3.6			
H.R.	3.0	33.0	7.05	.555	3.6	Keeper	.92	.99
H.R.	2.5		7.78	.490	4.30			
H.R.	3.0	27.0	7.55	.555	3.5	Keeper	.91	.82
3.75	2.0		8.38	.609	4.0			
5.5	4.0	32	8.24	.474	4.10	Keeper	.64	1.01
H.R.	3.0		7.30	.555	3.87			

TABLE 3-6

ARGON ELECTRON EFFICIENCY

Anode Type	Spacing Magnet Pole Surface (mm)	Potential Difference Between Keeper and Main Discharge (volts)	Electron Current per Ion Beam Ratio	Total Mass Flow (amps-equiv)	Main Discharge Current (amps)	Baffle Potential	Change in Exposed Wall Area	Corrected Electron Current per Ion Beam
H.R.	3.0	38.0	5.0	1.036	3.20	Keeper	0.91	0.91
3.75	2.0		5.0	1.228	4.25		0.64	1.27
5.5	4.0	40.0	7.17	0.984	5.0	Keeper	0.64	1.27
H.R.	3.0		5.65	1.036	4.0			

column is the electron per beam ion current ratio from the electron efficiency equation. Electron efficiency listed in the column, "Corrected Electron Current Per Ion Beam," is corrected for the differences in mass flow and discharge electron current. These corrections are calculated using the empirical equation presented below (Eq. 10).

The "Change in Exposed Wall Area" column lists the calculated change in magnet surface exposed to the discharge plasma due to changes in anode geometry or change in the width of the area defined by the hybrid radius-anode placement. The charge in magnet surface area defined by the two angles of the anode geometries being compared were assumed to constitute the change in exposed surface area as shown in Figure 3-5. The calculations were based on changes in the angle, θ, subtended by the normal to the discharge chamber wall and the line joining the center of the magnet cross-section to the edge of the adjacent anode. The ratio listed in the tables was arranged so the anode configuration with the smaller exposed magnet area was listed first.

The anode geometries were compared at equal, anode minus keeper, potentials. However, differences in arc impedance due to changes in the magnetic field made it impossible to select an operating point that had equal mass flow rates and arc currents as well. Correction factors were used to compensate for the differences.

Mass flow and arc current correction were included in the calculations to correlate data taken at slightly different operating parameters. The mass flow correction was empirical derived from changes in the average electron efficiency of three different test configurations due to changes in mass flow rates. The average empirical correction was equal to:

$$\eta_e = \frac{\eta_{el}}{\eta_{es}} \left(1 + \frac{m_L - m_S}{m_L}\right) \tag{10}$$

where η_{el} and η_{es} were the electron efficiency associated with the large and small mass flow rates m_L and m_S, respectively.

The discharge current difference corrections were calculated from the difference in the arc current divided by the greater current. The correction assumes electron ionization efficiency would decrease if the arc current density is reduced at the same operating potential and equivalent mass flow rates.[3] Reduction in arc current, assuming a fixed percentage of primary electrons, would reduce the ionization probability as a function of the change in electron density at the selected mass flow rate and operating potentials. As the relationship between ionization probability and electron current is linear [12] the effective impact of differences in arc current can be approximated by the ratio of the currents, more succinctly:

$$\text{Discharge Current Difference Correction} \sim \frac{\eta_{EG}}{\eta_{ER}} \frac{I_G - I_R}{I_G} \tag{11}$$

where I_G and I_R were the greater and reduced arc currents minus the uncorrected ion beam and η_{EG} and η_{ER} were the electron efficiencies associated with respective arc currents. It should be noted the larger and smaller discharge currents were not necessarily associated with the large and small mass flow rates.

The electron efficiency calculations listed in Tables 3-5 and 3-6 illustrate several interesting features of hemi thruster operation. Best hemi thruster performance was obtained with half round boundary

anodes located 3.0 mm average displacement from the MPS. Xenon operational characteristics listed in Table 3-5 compare test results with half round anodes 3.0 mm from the MPS against other anode types and placement test results. The first three sets listed in the table were taken from tests conducted with the anodes located closer than 3.0 mm from the MPS. The fourth compares the 3.0 mm results against results from tests with 5.5 mm wide anodes that were located further than 3.0 mm from the MPS. The predicted loss of electron efficiency listed under the wall ratio heading shows fairly good agreement with the test results shown in the corrected electron/ion beam column when the anodes were located closer than 3.0 mm from the MPS. Conversely, calculated and experimental results disagree when the anodes were moved beyond 3.0 mm from the MPS. These results implied the ion loss from the discharge chamber was increasing faster than possible gains in electron efficiency from diffusion path changes when the anodes were located closer than 3.0 mm from the MPS and the magnet-anode edge angles were greater than $\sim$ 0.6 radians. The inverse was implied when the anodes were further than 3.0 mm from the MPS.

Argon operation was unstable[4] when the anodes were located closer than 2.0 mm from the MPS thus limiting the amount of test data available for comparison. However, the two sets of recorded argon results support the xenon results; that is, increases in the magnet surface produced by anode geometry changes reduced electron ionization efficiency if the anodes were located closer than 3.0 mm from the MPS.

3.3 DISCHARGE PLASMA AND BEAM PROBE

3.3.1 DISCHARGE PLASMA

Tables 3-7, 3-8, and 3-9 list the plasma distribution and operating characteristics of the baseline and other cathode baffle-magnet

TABLE 3-7

HEXAGONAL THRUSTER ARGON OPERATION
DISCHARGE CHAMBER PLASMA DISTRIBUTION

TEST CONFIGURATION	BAFFLE		eV ion	MASS EFFICIENCY (percent)	ANODE NUMBER	RELATIVE PLASMA DENSITY IN ANODE PLANE			POTENTIAL DIFFERENCE BETWEEN ANODE AND KEEPER (volts)	PRIMARY ELECTRON ENERGY IN ANODE PLANE (eV)	PRIMARY-TO-MAXWELLIAN ELECTRON DENSITY RATIO IN ANODE PLANE		
	DIAMETER (cm)	POTENTIAL				Distance from Centerline (cm)					Distance from Centerline (cm)		
						1.0	2.75	4.5			1.0	2.75	4.5
BASELINE	1.1 (solid)	cathode	303	77.0	2	0.67	0.76	0.66	28	24	0.23	0.22	0.24
					3	1.0	0.81	0.736		23	0.15	0.17	0.18
					4	0.72	0.57	0.59		24	0.22	0.22	0.21
SMALL MAGNET	1.3 x 0.8 (annulus)	keeper	309	67.0	2	1.0	0.80	0.80	20	17	0.48	0.44	0.48
					3	0.72	0.65	0.65		19	0.31	0.32	0.32
					4	0.61	0.67	0.61		20	0.30	0.32	0.30
SMALL MAGNET	1.5 x 0.47 (annulus)	keeper	389	71.0	2	0.99	0.88	0.79	28	20	0.36	0.39	0.40
					3	1.0	0.87	0.87		22	0.23	0.24	0.24
					4	0.67	0.67	0.77		22	0.39	0.39	0.38
LARGE MAGNET	1.5 x 0.47 (annulus)	cathode	344	68.9	2	1.0	0.94	0.79	29	24	0.24	0.23	0.31
					3	0.98	0.90	0.74		27	0.28	0.28	0.36
					4	0.70	0.61	0.49		32	0.28	0.28	0.26

TABLE 3-8

HEXAGONAL THRUSTER XENON OPERATION
DISCHARGE CHAMBER PLASMA DISTRIBUTION

TEST CONFIGURATION	BAFFLE DIAMETER (cm)	BAFFLE POTENTIAL	eV Ion	MASS EFFICIENCY (percent)	ANODE NUMBER	RELATIVE PLASMA DENSITY IN ANODE PLANE — Distance from Centerline (cm) 1.0	2.75	4.5	POTENTIAL DIFFERENCE BETWEEN ANODE AND KEEPER (volts)	PRIMARY ELECTRON ENERGY IN ANODE PLANE (eV)	PRIMARY-TO-MAXWELLIAN ELECTRON DENSITY RATIO IN ANODE PLANE — Distance from Centerline (cm) 1.0	2.75	4.5
BASELINE	1.1 (solid)	cathode	284	93.4	2	0.95	0.82	0.82	25	22	0.14	0.16	0.16
					3	1.0	0.83	0.83		22	0.24	0.26	0.26
					4	1.0	0.87	0.83		22	0.18	0.20	0.21
SMALL MAGNET	.3 x 0.8 (annulus)	keeper	312	93.0	2	1.0	0.87	0.87	17	16	0.59	0.38	0.40
					3	0.68	0.61	0.62		16	0.39	0.39	0.42
					4	0.69	0.62	0.69		17	0.39	0.39	0.39
SMALL MAGNET	.5 x 0.47 (annulus)	keeper	236	91.4	2	0.99	0.93	0.85	20	18	0.25	0.24	0.25
					3	1.0	0.91	0.91		19	0.22	0.22	0.22
					4	0.72	0.72	0.86		21	0.24	0.24	0.25
LARGE MAGNET	.5 x 0.47 (annulus)	cathode	325	93.0	2	0.92	0.92	0.75	21	21	0.20	0.15	0.16
					3	1.0	0.91	0.77		23	0.16	0.17	0.17
					4	0.86	0.80	0.68		24	0.16	0.16	0.16

TABLE 3-9

HEXAGONAL THRUSTER MIXED MODE OPERATION
(Xenon Main Flow)
DISCHARGE CHAMBER PLASMA DISTRIBUTION

TEST CONFIGURATION	BAFFLE		eV ion	MASS EFFICIENCY (percent)	ANODE NUMBER	RELATIVE PLASMA DENSITY IN ANODE PLANE			POTENTIAL DIFFERENCE BETWEEN ANODE AND KEEPER (volts)	PRIMARY ELECTRON ENERGY IN ANODE PLANE (eV)	PRIMARY-TO-MAXWELLIAN ELECTRON DENSITY RATIO IN ANODE PLANE		
	DIAMETER (cm)	POTENTIAL				Distance from Centerline (cm)					Distance from Centerline (cm)		
						1.0	2.75	4.5			1.0	2.75	4.5
BASELINE	1.1 (solid)	cathode	207	90.3	2	1.0	0.97	0.82	27	24	0.20	0.21	0.18
					3	0.78	0.63	0.63		26	0.26	0.28	0.28
					4								
SMALL MAGNET	1.3 x 0.8 (annulus)	keeper	375	81.0	2	1.0	0.65	0.67	21	15	0.32	0.40	0.43
					3	0.73	0.69	0.69		17	0.39	0.38	0.38
					4	0.72	0.56	0.72		19	0.39	0.35	0.39
SMALL MAGNET	1.5 x 0.47 (annulus)	keeper	334	84.0	2	1.0	0.76	0.74	22	23	0.20	0.25	0.25
					3	0.80	0.80	0.80		24	0.26	0.26	0.26
					4	0.76	0.76	0.85		26	0.24	0.23	0.23
LARGE MAGNET	1.5 x 0.47 (annulus)	cathode	224	80.0	2	0.97	0.97	0.81	24	26	0.17	0.17	0.19
					3	0.96	0.96	0.78		25	0.15	0.15	0.18
					4	1.0	1.0	0.67		25	0.13	0.13	0.18

configurations tested with argon, xenon, and mixed mode (xenon main flow), respectively, in the 12 cm hex MESC thruster. The "relative plasma density" values were calculated from the Langmuir probe data electron densities at the indicated spatial points versus the maximum indicated total electron density recorded with that particular cathode configuration.

Langmuir probe data were reduced after the method of Strickfaden and Geiler[13]. The test results listed in the three tables show the hex thruster plasma characteristics were impacted by changes to the cathode magnet-baffle. A comparison of the values listed under the main and keeper potential difference and the primary electron energy shows fair experimental agreement between these two potentials for all cases tested. For example, argon tests with the 2.3 cm magnet and a single tube baffle support tube and 1.3 x 0.8 cm annular baffle, had a 20 volt potential difference and a primary electron energy of 17 to 20 volts. Changing to a 3.3 cm magnet and double tube cathode magnet-baffle configuration increased the potential difference to 29 volts and the primary electron energy from 24 to 32 volts. The plasma characteristics in Tables 3-7, 3-8, and 3-9 for the above two test configurations show that the cathode magnet-baffle change redistributed the discharge plasma axial and radial densities. The small magnet, annular baffle configuration produced a non-uniform radial distribution in the plane of the second anode and fairly uniform plasma distribution in the planes of the third and fourth anodes. The large, 3.3 cm magnet configuration produced a plasma which was fairly uniform 1.0 and 2.75 cm from the centerline in the plane of all three anodes but fell off 20 percent 4.75 cm from the centerline.

Comparison of the relative densities of primary-to-Maxwellian electrons in the same two magnet-baffle configurations, showed the 2.3 cm magnet produced a greater overall ratio of primaries than did the large magnet for all three propellents. The relative densities were found to vary somewhat with propellent. Xenon tests with the 2.3 cm magnet were found to have a greater density 1.0 cm from the centerline in the plane of anode number two, whereas mixed mode operation had the minimum relative density at the same point.

3.3.2 BEAM PROBE

Faraday probe data were collected at two points downstream of the accel by moving three probes through the beam cross section. Two of the three probes used to measure ion beam distribution were located 22 cm downstream of the accel grid.

Tables 3-10, 3-11, and 3-12 are selected samples of calculated results from 22 cm downstream probe test data with various cathode magnet-baffle configurations at different operating parameters. In general, annular baffle tests produced a more peaked ion distribution and wider beam spread half angle than comparable tests with a solid baffle disk. As seen in table 3-10, argon operation with solid disk cathode potential baffle, baseline configuration, produced a beam flatness of 0.64 and beam spread half angle of 24 degrees with a beam current density of 7.1 mA/cm^2 at a net potential of 840 volts and net-total potential ratio of 0.67. With an annular baffle and the same magnet and operating conditions, a beam flatness of 0.62 and beam spread half angle of 26 degrees were obtained. Similar results were obtained with xenon operation in both the unmixed and mixed mode (xenon main flow).

TABLE 3-10

ARGON FARADAY CUP PROBE DATA

Baffle Configuration	Net Potential (volts)	Net-Total Potential (ratio)	Beam Current Density (amps x 10^{-3})	Beam Flatness	Beam Spread Half Angle (degree)
Herc Thruster Annular Baffle Keeper Potential	600	.55	4.8	.60	22
Hex Thruster 3.3 cm Dia. Magnet Annular Baffle Keeper Potential Large Dia. Main Feed	840	.68	7.0	.57	26
Hex Thruster 3.3 cm Dia. Magnet Annular Baffle Cathode Potential Large Dia. Main Feed	840	.68	7.2	.58	26
Hex Thruster 2.3 cm Dia. Magnet Annular Baffle Keeper Potential Small Dia. Main Feed	840	.63	7.0	.62	26
Hex Thruster 2.3 cm Dia.Magnet Annular Baffle Keeper Potential Small Dia.Main Feed	840	.67	6.5	.64	26
Hex Thruster Baseline: Solid Baffle Cathode Potential	840	.67	7.1	.64	24

TABLE 3-11

XENON FARADAY CUP PROBE DATA

Baffle Configuration	Net Potential (volts)	Net-to-Total Potential (volts)	Beam Current Density (amps x 10^{-3}	Beam Flatness	Beam Spread Half Angle (degree)
Hex Thruster 3.3 cm Magnet Annular Baffle Cathode Potential Large Main Feed	1000	.72	5.0	.79	24
Hex Thruster 3.3 cm Magnet Annular Baffle Keeper Potential Large Mainfeed	1000	.72	5.0	.72	24
Hemi Thruster Annular Baffle Keeper Potential	600	.56	5.1	.78	25
Hex Thruster Baseline: Solid Baffle Cathode Potential	1100	.79	5.0	.88	22
Hex Thruster Baseline: Solid Baffle Cathode Potential	1000	.72	3.6	.88	21

TABLE 3-12

DUAL GAS FLOW

XENON MAIN FLOW FARADAY CUP PROBE DATA

Baffle Configuration	Net Potential (volts	Net-to-Total Potential (volts)	Beam Current Density (amps x 10^{-3})	Beam Flatness	Beam Spread Half Angle (degree)
Hex Thruster 3.3 cm Magnet Annular Baffle Keeper Potential Large Main Feed	1100	.730	6.9	.626	26
Hex Thruster 3.3 cm Magnet Annular Magnet Keeper Potential Large Main Feed	880	.638	7.4	.603	23
Hex Thruster Baseline Solid Baffle Cathode Potential	1100	.74	6.8	.73	22

The solid baffle tests also produced a "hollow beam" ion distribution where peak current density occurred at points 3.2 cm on either side of the ion source axis. Annular baffles, tested with either size magnet and main feed produced a more peaked beam.

SECTION 4

DISCUSSION OF TEST RESULTS

4.1 12 CM HEXAGONAL MESC THRUSTER TESTS

4.1.1 IMPLICATIONS OF THE INERT GAS TEST RESULTS

Cathode baffle changes made a major impact on the hex thruster inert gas operating parameters. Replacing the cathode-potential-solid-disk baffle with a keeper-potential-annulus reduced the thruster anode potential 10 volts. Operation with xenon at 29 volts anode potential produced 80 percent mass utilization efficiency with a 20 percent increase in discharge chamber total eV/ion compared to disk baffle operation. The resultant reduction in plasma potential should reduce discharge chamber sputtering and help to extend thruster lifetime.

Relocating the point of introduction of the main feed gas flow produced little change in thruster performance. The main gas flow was originally fed into the discharge chamber through holes in a 1.3 cm radius ring concentrically located about the cathode magnet. Replacing this main flow ring with three tubes 2.6 cm from the thruster centerline constituted a radical configuration change. Therefore, in 12 cm MESC thruster with a discharge chamber length-to-diameter ratio of approximately 0.75 and small hole accel grid ion optics, the thruster performance is believed to be independent of the mode of propellent injection along the rear wall of the discharge chamber.

4.1.2 HEXAGONAL MESC THRUSTER PERFORMANCE IMPROVEMENTS

Further improvements in hex MESC thruster performance can be realized through subtle changes to the discharge chamber geometry. For example, modifications to the cathode baffle reduced the anode operating potential and hence is a possible method of extending thruster lifetime. The change in axial plasma density produced off-optimum performance by reducing current density uniformity among the anode collecting the majority of the discharge current. Reoptimization of the anode placement to obtain uniformity should retain the low potential discharge operation while reducing discharge eV/ion.

Thruster test results indicated some reduction in discharge energy consumption could be realized by careful anode-to-magnet positioning. Variation in the peripheral magnetic field arises from difference in the residual field of the individual magnets and the geometry of the discharge chamber. Adjusting the anodes to compensate for the differences in the magnet residual field would produce a more homogeneous electron current distribution to most of the anodes and a subsequent reduction in eV/ion. However, these performance improvements are limited by the corner and end magnetic fields effects on discharge chamber plasma distribution.

4.1.3 HEXAGONAL MESC THRUSTER PERFORMANCE LIMITATIONS

The design of the hexagonal thruster limited the ultimate performance that could be obtained from this discharge chamber. The sides of the discharge chamber intersecting the rear wall at right angles produced a nonuniform magnetic field at each angular interface.

The 120 degree angle between sections of the same hexagonal magnet ring produced a very strong magnetic field over the anodes within a few millimeters of the corners. Similarly, the 90 degree junction

between the side and rear walls of the discharge chamber structure isolated the corner anodes from the discharge plasma. A possible loss mechanism in the plasma at the corners is postulated as follows.

Ionization probability is directly proportional to electron current density.[3] Electron current densities to the two upstream corner anodes averaged ~ 10 percent of the typical anode densities current. The less-than-average electron currents were caused by a 40 percent greater-than-average magnetic flux at the anode surface produced by the 90 degree magnet-corner geometry. Hence, the magnetic field at the corner anodes reduced the Bohm electron diffusion and reduced the ionization probability near the anodes. However, the large magnetic fields at the corner anode surfaces, B_A, did not effect the ionic hybrid radii as the anode-magnet geometry and pole face magnetic field, B_p, were similar throughout the discharge chamber. In summary, the corners were regions of low ionization probability and hence low plasma density with enhanced ion diffusion and wall recombination losses. The discharge chamber corners effects could be minimized by smoothing out the angular interfaces in the discharge chamber, i.e., use of a hemispherical design.

4.2 PLASMA PROPERTIES

4.2.1 THRUSTER PERFORMANCE CORRELATION

Hex thruster cathode baffle modifications produced changes in the discharge plasma distribution and primary-to-Maxwellian electron ratio that effected hex thruster performance. Optimum thruster performance was produced with a cathode potential disk type baffle and a fairly uniform radial plasma distribution. The plasma distribution of the optimum baffle performance configuration had less than 12 percent variation in radial plasma density across the plane of the second

anode from the grids. Downstream beam profile measurements found the same configuration had a flatness coefficient of 0.64 for argon operation and 0.84 for xenon. A maximum in the axial plasma density profile was located 1.3 cm downstream of the midpoint of the chamber length.

Use of a small, keeper potential, annular baffle increased the radial density differences from 12 to 20 percent or more. The change also increased the primary-to-Maxwellian electron ratio by a factor of two and shifted the axial plasma maximum toward the grids. The keeper potential annular baffle configuration also reduced the xenon plasma operating potential ~10 volts.

Replacing the small keeper potential annular baffle with a larger one produced similar test results. Compared to the optimum baffle configuration operation, the radial plasma density was slightly more uniform and the axial density moved slightly upstream in the discharge chamber. The large cathode baffle configuration had a beam flatness coefficient of 0.57 and 0.72 for argon and xenon, respectively, and increased the discharge eV/ion above the optimum performance value.

Tests with the annular baffle configurations consumed more discharge energy than the optimal configuration due to changes in the plasma density gradient. The high plasma concentrations in the central region of the discharge chamber increased the density gradient and the resultant Bohm electron diffusion to the anodes and degraded performance. The uneven plasma distribution could probably be reduced by re-positioning the anodes.

Optimum hex thruster performance was produced when the discharge chamber anodes were located a uniform distance from the magnet pole surface (MPS). Anode electron current density measurements found fairly equal current densities were collected by the anodes in the

optimum placement configuration. The upstream corner anodes and the anode adjacent to the grid (number one) were the exceptions and collected less than the average density. The corner anodes collected $\sim$ 10 percent of the average electron current density, and anode one collected 66 percent of the average current. Relocating the first anode into the discharge, farther from the MPS, increased the discharge energy consumption and reduced thruster performance. The corner anodes could not be moved far enough from the MPS to achieve the average current due to geometry constraints inherent in the discharge chamber design.

4.2.2 PLASMA DENSITY DISTRIBUTION MODIFICATIONS

Plasma distribution within the discharge chamber was a function of three interacting features of the discharge chamber geometry. The test results above indicated the cathode baffle geometry can play a major role in determining plasma axial and radial distribution. Similarly, relocating the boundary anodes with respect to the MPS appears to modify the axial plasma distribution and to a lesser extent the radial density. These changes, plus changes to the cathode magnet determine the axial and radial plasma distribution in the discharge.

Anode effects on plasma distribution stem mainly from space charge neutrality requirements. Moving one anode ring into the discharge and a lower peripheral magnetic field increases the diffusion current to that anode. The increased loss of electrons from the plasma produces a flow of both electrons and ions into the plasma zone adjacent to the anode and shifts plasma density toward the anode. This shift can be modulated by changes in the cathode geometry.

Cathode magnetic field changes redistributed the radial and axial plasma density. If the cathode magnet was moved farther into the discharge region, the axial density distribution was shifted downstream a similar amount. The shift in plasma distribution increased the electron diffusion current to the downstream anodes. The inverse was true when the cathode magnet was moved out of the discharge. Again, this redistribution can be modulated by baffle and anode changes.

Achieving optimum thruster performance with these interactions by controlling the discharge plasma distribution was a relatively straightforward procedure. The cathode magnet was positioned to null the axial magnetic field while the anodes were located in a uniform magnet field for inert gas operation. This particular cathode magnet-anode positioning produced the best performance with a baseline baffle structure.

4.3 12 CM HEMISPHERICAL THRUSTER

4.3.1 DISCUSSION OF PRELIMINARY HEMI THRUSTER TEST RESULTS

Measurement of the actual hemi MESC peripheral field found it deviated markedly from the ideal MESC design. The point-to-point field at the anodes positioned for inert gas operation differed by as much as a factor of two in a discontinuous fashion.

The thruster operation with the nonuniform field produced wide differences in anode current density over a short azimuthal length of the same anode. Attempts to optimize performance by moving the anodes closer to the MPS concentrated the electron current to low field sections of the anodes. To overcome the electron current concentration, the anodes were repositioned in a quasi-uniform peripheral magnetic field. Greater anode field uniformity was achieved by locating sections of the anodes different distances from the MPS.

Test data indicated anode-MPS spacing less than 3.0 mm apparently increased ionic wall recombination losses. Moving the anodes farther from the MPS decreased the electron diffusion path length reducing discharge chamber performance. The former anode positioning limited the ultimate mass efficiency while the latter increased discharge chamber eV/ion at all mass utilization efficiencies. These hemi thruster performance restrictions appeared to be caused by the magnetic field.

4.3.2 IMPROVEMENTS IN THE HEMISPHERICAL MESC THRUSTER PERFORMANCE

Clearly, hemi test results indicate thruster performance can be improved by replacing the existing nonuniform magnetic field with a more uniform peripheral field. The Platcover magnets in the existing hemi design have a high energy product (BH), 8 Meg Gauss-Oersteds (MGOe) and high coercive force. The replacement magnets would need to have a greater energy product and fit within the dimensional limitations of the existing hemi design.

SECTION 5

CONCLUSIONS

5.1 GENERAL CONCLUSIONS

This effort has provided significant insight into the inert gas operation of the MESC discharge chamber and reaffirmed previously reported excellent performance. Tests with two generations of 12 cm MESC thrusters established relationships between discharge chamber operating characteristics and thruster performance.

5.2 HEXAGONAL 12 CM MESC THRUSTER

The hex thruster tests demonstrated that thruster operation was effected by changes to the cathode baffle, cathode magnet and boundary anode magnet field. These three interacting elements of the discharge chamber defined its performance. Changes in the discharge chamber elements caused detectable changes in plasma distribution and thruster performance.

The MESC discharge chamber operation depended on the plasma distribution within the discharge. Xenon and argon plasma uniformity close to the extraction grids produced better performance, in terms of lower eV/ion and greater mass utilization, than did thruster operation with a nonuniform radial distribution in the same region.

Variations of the cathode baffle were found to be particularly interesting. Switching from a cathode potential disk to a keeper potential annulus style baffle reduced the anode operating potential 10 volts with no loss in mass utilization efficiency. Reduction in

operating potential resulted from increasing the ratio of Maxwellian-to-primary electrons and maintaining primary electron temperature. The baffle structural change reduced the keeper plasma potential 10 volts as well and maintained the potential difference between the keeper and main plasmas. Operation at the lower anode/discharge potential would significantly extend thruster lifetime by reducing ionic sputtering. The small loss in performance associated with these changes could be minimized by reoptimizing the anode-magnet field positioning.

Changing the baffles produced a small reduction in performance due to changes in the axial and radial distribution of the discharge plasma. The axial distribution of anode electron current densities were found to modulate the axial distribution of the discharge plasma. Reducing the peripheral magnetic field at a single anode increased the plasma density in the region adjacent to the anode. The inverse was true with increases in the anode magnetic field.

Cathode magnet geometry also impacted radial and axial plasma distribution. Increasing the cathode magnet flux density shifted the discharge plasma toward the grids and increased the on-axis density. Reducing the field shifted the plasma distribution upstream.

5.3 HEMISPHERICAL 12 CM MESC THRUSTER

The hemi thruster tests confirmed the necessity of a high flux density, uniform peripheral magnetic field to achieve good thruster performance. Hemi thruster peripheral magnets had an average flux density that was 60 percent of the hex thruster magnets. The hemi thruster anode peripheral magnetic field varied from point-to-point by a

factor of two because of magnetization abnormalities in both direction and magnitude. Preliminary hemi thruster tests found it was impossible to achieve performance comparable to the hex thruster due in part to magnetic field differences.

Hemi thruster xenon performance mapping with variable anode-magnet geometries to compensate for peripheral field differences found performance improvements were limited by ionic wall losses. Close anode-magnet spacing compatible with inert gas operation or use of narrower anodes parallel to the chamber walls reduced the maximum attainable xenon mass utilization efficiency. The reduction in efficiency appeared to be coupled to increases in the magnet surface area not masked by the anodes.

Hemi thruster argon test results were limited in the ultimate mass utilization efficiency compared to the hex thruster results. These limitations appeared to be caused by increased wall recombination losses and a calculated ionization mean free path of the same order as the hemi discharge chamber length.

5.4 ON-GOING EFFORT

More hemi thruster tests are to be conducted using different anode geometries and magnets more suitable for inert gas operation and using several different discharge chamber lengths. The existing hemi discharge chamber is being fitted with samarium-cobalt magnets. This change consists of removing the present Platcovar magnets, filling the groove in the discharge chamber wall with an iron spacer and mounting the samarium-cobalt magnets in place. Substituting the rare

earth magnets should increase the peripheral magnetic field and improve its uniformity to the 10 percent point-to-point variations seen in the hex thruster. Discharge chamber length will be varied by attaching 2.3 cm long chamber sections to the grid mounting flange of the discharge chamber. Additional samarium-cobalt magnets will be used in the extensions. Tests will be conducted with at least three different discharge chamber lengths.

APPENDIX A

MIXED MODE BEAM CURRENT DOUBLE CHARGED ION CORRECTION

The equivalent single charged beam current, I_B, is defined as

$$I_B = I_+ - |I_-| - \frac{I^{++}}{2}$$

where I_+ is the screen grid positive high voltage supply current; $|I_-|$ the absolute value of the accel grid supply current; and I^{++} the double charged ion current.

The percentage of double charged ion beam current, I^{++}/I^+, can be found by direct measurement or taken from previous test data under similar operating conditions. In the case of "mixed mode" operation, direct measurement is virtually ruled out due to the complexity of the ion beam components. However, test data for single gas operation can be used to establish the percentage of double charged current present in the beam under a variety of operating conditions. The double charged current for a single gas is:

$$\frac{I^{++}}{I^+ + I^{++}} = f(\Delta V)$$

As $$I_+ = I^+ + (I^+ + I^{++})$$

$$\frac{I^{++}}{I_+} = f(\Delta V)$$

where I^{+} and I^{++} are the single and double charged ion components of the screen grid current I_{+}, and $f(\Delta V)$ is the functional relationship between double ion current and discharge operating parameters.[14] The screen grid current can also be expressed as a function of discharge operating parameters for single gas operation:

$$I_{+} = n_{o} f)D)$$

and

$$n_{o} = \Gamma(\epsilon)\ \dot{M}$$

so

$$n_{o} \propto \dot{M}$$

and

$$I_{+} \sim \dot{M}\ f(D)$$

where n_{o} is the spatial density of the neutral gas; $\Gamma(\epsilon)$, the neutral distribution function; $f(D)$, the total ionization probability as a function of discharge parameters for that species; and $\dot{M}$, the neutral gas mass flow rate. During mixed mode operation, the double charged ion current can be expressed as:

$$I^{++} = I_{A}^{++} + I_{Xe}^{++} = I_{+A}\ f(\Delta V)_{A} + I_{+Xe}\ f(\Delta V)_{Xe}$$

where I_{A}^{++} and I_{Xe}^{++} are the argon and xenon double charged ion current components of the grid supply current, respectively; I_{+A} and I_{+Xe}, the argon and xenon components of the grid current, respectively; and $f(\Delta V)_{X}$ the double charged ion function for the two gases. Assuming complete mixing of the two gases, the single gas flow rate is replaced with the fraction of the individual species present in the total flow during mixed mode operation:

$$I^{++} \sim \frac{\dot{M}_A}{\dot{M}_A + \dot{M}_{Xe}} f(D)_A \; f(\Delta V)_A + \frac{\dot{M}_{Xe}}{\dot{M}_A + \dot{M}_{Xe}} f(D)_{Xe} \; f(\Delta V)_{Xe}$$

where $\dot{M}_A$ and $\dot{M}_{Xe}$ are the respective argon and xenon mass flow rates into the discharge chamber; $f(D)_A$ and $f(D)_{Xe}$, the total ionization probability for argon and xenon, respectively; and $f(\Delta V)_A$ and $f(\Delta V)_{Xe}$, the double ion production for argon and xenon, respectively. Total ionization probability, $f(D)_X$, is taken from single gas operation data as a function of discharge parameters versus the ratio of $I_+/\dot{M}$.

APPENDIX B

GENERALIZED PROPULSION EFFICIENCY

An ideal thruster accelerates its exhaust to a uniform velocity to generate thrust. Exhaust power and thrust are given by

$$P = \frac{1}{2} \dot{M} v^2$$

$$T = \dot{M} v$$

where $\dot{M}$ is the mass flow rate and v the mass velocity. Substituting:

$$T^2 = 2 \dot{M} P$$

If the device is non-perfect, $\dot{M}$ is replaced by $\eta_M \dot{M}$ and P replaced by $\eta_p P$. Substituting:

$$T^2 = 2\eta_M \eta_p \dot{M} P$$

If the velocity is not the same for all particles, the thruster power and thrust become:

$$T = \eta_M \dot{M} \bar{v}$$

$$\eta_p P = \frac{1}{2} \eta_M \dot{M} \overline{v^2}$$

where $\bar{v}$ is the average particle velocity and M the ionic mass. In an ion thruster the individual particle velocity is:

$$v = \left(\frac{2qV}{M}\right)^{1/2}$$

where q is the electron charge and V the accelerating electrostatic potential and M the ionic mass. The overall efficiency can be defined as:

$$\frac{T^2}{2\dot{M}P} = \eta_M \eta_P \frac{\bar{v}^2}{\overline{v^2}}$$

Thus, the "distributed efficiency" associated with nonuniform velocity is defined as:

$$\eta_d = \frac{\bar{v}^2}{\overline{v^2}}$$

In the specific case where there are two species having different charge-to-mass ratios, the distribution efficiency is:

$$\bar{v} = (2V)^{1/2} \left[(f_1 (q/M)_1^{1/2} + f_2 (q/M)_2^{1/2} \right]$$

$$\overline{v^2} = 2V \left[f_1 (q/M)_1 + f_2 (q/M)_2 \right]$$

where $f_1 = \frac{\dot{M}_1}{\dot{M}_1 + \dot{M}_2}$ and $f_2 = \frac{\dot{M}_2}{\dot{M}_1 + \dot{M}_2}$

so $$\eta_d = \frac{\left[f_1 (q/M)_1^{1/2} + f_2 (q/M)_2^{1/2} \right]^2}{f_1 (q/M) + f (q/M)}$$

where $(q/M)_1$ and $(q/M)_2$ are the charge-to-mass ratio of the two species of f_1 and f_2 the associated mass flow fraction of the species.

REFERENCES

1. Ramsey, W.D., "Inert Gas Ion Source Program", NASA CR-159423, July 1978.

2. Guthrie, A., Wakerling, R.K., "The Characteristics of Electrical Discharges in Magnetics Fields", McGraw-Hill Book Company, Inc, 1949.

3. Chen, Francis F., "Introduction to Plasma Physics", Plenium Press, 1974.

4. Kaufman, Harold R., "Inert Gas Thrusters", NASA CR-159527 November 1978.

5. Robinson, R.S., "Thirty cm Ion Source", Industrial Ion Source Technology (H.R.Kaufman, ed.) NASA Contr. Rep. CR-135149, Nov. 1976.

6. Haines, M.G., "Plasma Containment in Cusp-Shaped Magnetic Field", Nuclear Fusion 17, 4, 1977.

7. Leung, K.N., Hershkowitz, Noah, and Mackenzie, K.R., "Plasma Confinement by Localized Cusps", The Physics of Fluid, Vol. 19 No. 7, July 1976.

8. Kitsunezaki, A., Tanimoto, M., and Sediguchi, T., Phys Fluids 17, 1974.

9. Moore, R. David, "Magneto-Electrostatically Contained Plasma Ion Thruster", AIAA paper No. 69-260, AIAA 7th Electrical Propulsion Conference, Williamsburg, VA, March 1969.

10. James, E.L., and Ramsey, W.D., "A Prototype North-South Station-keeping Thruster", AIAA paper No. 74-1119, AIAA/SAE 10th Propulsion Conference, San Diego, CA., October 1974.

11. Hunter, R.V., REH Engineering, Private Communication.

12. Masek, T.D., "Plasma Properties and Performance of Mercury Ion Thrusters", AIAA paper No. 69-256, AIAA 7th Electric Propulsion Conference, Williamsburg, VA., March 1969.

REFERENCES

13. Strickfaden, W.P., and Geiler, K.L., "Probe Measurements of the Discharge in an Operating Electron-Bombardment Engine", AIAA Journal, Vol. 1, August 1963.

14. Peters, R.R., and Wilbur, P.J., "Mercury Ion Thruster Doubly Charged Ion Model", AIAA paper No. 76-1010, AIAA International Propulsion Conference, Key Biscayne, FL. Nov. 1976.

C-2